Available online at www.sciencedirect.com
ScienceDirect
Journal of Organometallic Chemistry 692 (2007) 93–110
Journal of Organometallic Chemistry
www.elsevier.com/locate/jorganchem

Ruthenium and chromium complexes bearing pH-indicators as the η^6-arene ligand: Synthesis, characterization, and protonation behavior

Miyuki Hirasa, Akiko Inagaki, Munetaka Akita *

Chemical Resources Laboratory, Tokyo Institute of Technology, R1-27, 4259 Nagatsuta, Midori-ku, Yokohama 226-8503, Japan

Received 23 May 2006; received in revised form 11 July 2006; accepted 18 July 2006
Available online 3 September 2006

Abstract

A series of ruthenium and chromium complexes bearing pH indicators as the η^6-arene ligand, $(\eta^6\text{-X})(ML_n)_y$ [X = methyl yellow, crystal violet lactone, phenolphthalein; $ML_n = RuCp^{*+}$, $RuCl_2(L)$, $Cr(CO)_3$; $y = 1, 2$] is prepared and characterized by spectroscopic and crystallographic methods. Of the plural arene rings in the indicators, a specific arene ring can be successfully coordinated to the metal center in a selective manner under appropriate conditions (i.e. use of the precursors of different oxidation states and reaction with the non-protonated and protonated pH indicator). The obtained indicator complexes show halochromic behavior depending on pH as observed for the parent molecules but the transition pH ranges are shifted to the more acidic side because of the attachment of the electron-withdrawing metal fragments, which decrease the basicity of the attached pH indicators.

Keywords: pH Indicators; η^6-Arene complex; Ruthenium; Chromium

1. Introduction

Organometallic species with an auxiliary, which is sensitive to the change of the environment, could be utilized as a functional sensor. Chromic compounds are characterized by their feature that they change their colors upon application of a stimulus such as light, heat, and pH change. The color change is induced by a remarkable change of their electronic structures, which would also trigger some new reactivity. Combination of these two systems would lead to a new chemical system such as a self-curing system (Scheme 1) [1].

In the present study, halochromic pH-indicators [2] were chosen as the chromic ligand [3], and we wish to report the results of synthesis and characterization of the ruthenium and chromium complexes bearing pH-indicators as the η^6-arene ligand. As typical examples of pH-indicators, azo dye (methyl yellow (MY; **1**)) and phthalein dye (crystal violet lactone (CVL; **2**) and phenolphthalein (PP; **3**)) were chosen and subjected to complexation with metal species. In Scheme 2, the coloring mechanisms of the dyes are shown.

Protonation of MY (**1**) promoted by the NMe_2 group occurs at the nitrogen atom bonded to the C_6H_5 ring ($[\mathbf{1}+H]^+$) to bring about contribution of the colored quinoidal form. On the other hand, protonation of the phthalein dye **A** bearing electron-donating substituents X (e.g. NMe_2 in **2**) or deprotonation of the phenol derivatives (e.g. X = OH (**3**)) induces heterolysis of the C–O bond of the lactone moiety. As a result, the π-systems separated by the central sp^3-carbon atom and localized on the three aromatic rings in the original form is spread over the three aromatic rings through the central sp^2-carbon atom to cause appearance of absorptions in the visible region, i.e. coloring (**B′**, **B″**, **C′**, **C″**, etc.).

Because most of organic chromic compounds consist of aromatic groups, we choose the $RuCp^*$, $RuCl_2(L)$, and $Cr(CO)_3$ fragments to be attached to them. The organometallic chemistry of the (η^6-arene)–ruthenium [4] and –chromium complexes [5,6] has been studied extensively and well established. While studies on interaction with alkali and

* Corresponding author.
E-mail address: makita@res.titech.ac.jp (M. Akita).

0022-328X/$ - see front matter © 2006 Elsevier B.V. All rights reserved.
doi:10.1016/j.jorganchem.2006.07.046

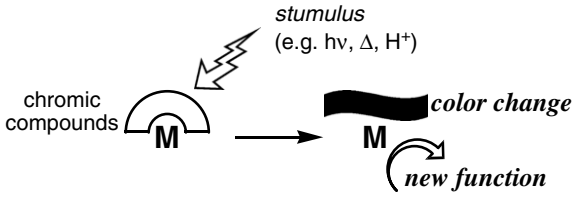

Scheme 1.

alkali earth metals appeared [7], no organo-transition metal species has been reported so far. The present study revealed (1) the capability of the pH indicators working as the η^6-ligands and (2) the modified functions of the adducts as the pH-sensitive molecules.

2. Results and discussion

2.1. Synthesis and characterization of pH-indicator complexes

2.1.1. Methyl yellow complexes

Azobenzene dyes constitute an important class of pH-indicators, and methyl yellow **1** was subjected to complexation with the Ru and Cr fragments.

2.1.1.1. Cationic RuCp complexes, [(η⁶-MY)RuCp*]PF₆ (5⁺ · PF₆) (MY = methyl yellow).* Reaction of **1** with the labile $RuCp^{*+}$ precursor, $[Cp^*Ru(NCMe)_3]PF_6$ (**4** · PF_6) [8], in CH_2Cl_2 gave an isomeric mixture of two mononuclear adducts **5a** · PF_6 and **5b** · PF_6 in 1:5 ratio (Scheme

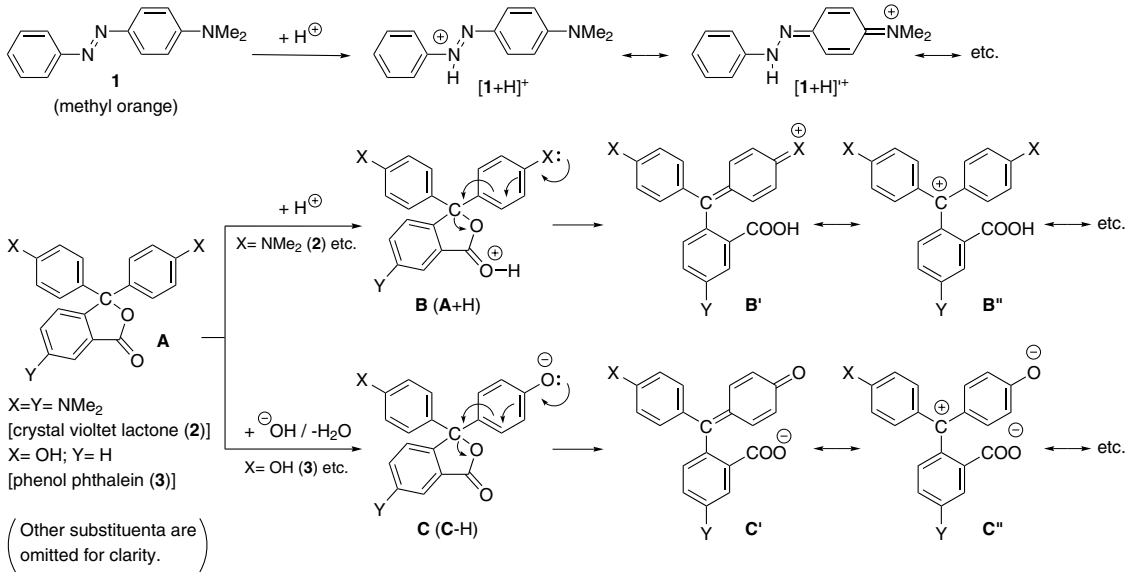

Scheme 2.

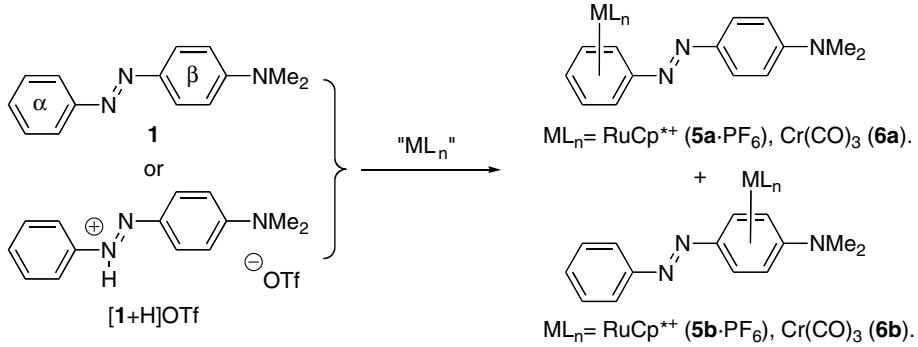

"ML_n" = $[RuCp^*(NCMe)_3]PF_6$ (**4**·PF_6) / CH_2Cl_2 / r.t.
$Cr(CO)_6$ / OBu_2 + THF / 120°C

ML_n	SM *	yield (%) **	ratio
$RuCp^*$	**1**	71	**5a**·PF_6 : **5b**·PF_6= 1 : 5
	[**1**-H]OTf	80	**5a**·PF_6 : **5b**·PF_6= 5 : 1
$Cr(CO)_3$	**1**	10	**6a** : **6b**= 1 : 5
	[**1**-H]OTf	0	-

* starting material. ** total yield.

Scheme 3.

Table 1
^{1}H NMR data for pH-indicator complexes[a,b]

Compound (solvent)	Cp*	Coordinated Ar	Non-coordinated Ar	NMe_2
5a · PF_6 (CD_2Cl_2)	1.88	6.40 (2H, d, 6.2), 5.97 (2H, m), 5.85 (1H, m)	7.86 (2H, d, 7.2), 6.76 (2H, d, 7.2)	3.13
5b · PF_6 (CD_2Cl_2)	1.94	6.23 (2H, d, 7.6), 5.51 (2H, d, 7.6)	7.7 (2H, m), 7.4 (3H, m)	
5a′ · PF_6 (CD_2Cl_2)	1.90	6.41 (1H, d, 6.4), 6.10 (2H, m), 6.04 (1H, d, 5.1)	7.76 (2H, d, 9.2), 7.38 (4H, m), 7.17–7.24 (6H, m), 7.03 (2H, d, 9.2)	
6a (acetone-d_6)		6.29 (2H, d, 6.8), 5.86 (2H, m), 5.70 (1H, m)	7.79 (2H, d, 9.4), 6.84 (2H, d, 9.4)	3.13
6b (acetone-d_6)	–	6.64 (2H, d, 7.6), 5.59 (2H, d, 7.6)	7.82 (2H, m,), 7.55 (3H, m)	3.06
7 · PF_6 (CD_3CN)	1.65	5.95 (2H, d, 6.7), 5.91 (2H, d, 6.7), 5.31 (2H, d, 6.7), 5.25 (2H, d, 6.7)	7.59 (1H, d, 8.4), 7.17 (1H, d, 8.6), 7.12 (1H, s), 6.86 (2H, d, 9.0), 6.61 (2H, d, 9.0)	3.03, 3.01, 2.87
8 · $(PF_6)_2$ (CD_3CN)	1.63	5.86 (2H, d. 6.8), 5.77 (2H, d, 6.8), 5.25 (2H, d, 6.8), 5.18 (2H, d, 6.8)	7.78 (1H, d, 9.6), 7.25–7.29 (2H, m)	3.07, 2.98
10 (C_6D_6)	–	5.66–5.62 (2H, m), 4.18 (1H, d, 5.7)	7.95 (2H, d, 8.8), 7.42 (2H, d, 8.8), 6.60 (2H, d, 9.0), 6.42 (2H, d, 9.0)	2.51, 2.45, 2.23
12 (DMSO-d_6)	–	5.36 (1H, s), 5.28 (1H, d, 6.8), 4.97 (1H, d, 6.8)	7.21–7.03 (8H, m)	~3.10 (br.)
13a ($CDCl_3$)	–	6.14 (1H, d, 6.1), 5.00 (1H, s), 4.67 (1H, d, 5.6)	7.70 (2H, d, 8.6), 6.99 (2H, d, 8.6), 6.71 (2H, d, 8.6), 6.55 (2H, d, 8.6)	3.30, 3.23, 2.95, 2.91
13b ($CDCl_3$)	–	6.31 (1H, d, 6.6), 5.30 (1H, d, 6.6), 4.76 (1H, s)	7.67 (2H, d, 8.3), 6.96 (2H, d, 8.3), 6.70 (2H, d, 8.5), 6.54 (2H, d, 8.3)	3.24, 2.93, 2.89
14a (CD_3CN)	–	5.51 (1H, d, 6.6), 4.63 (1H, d, 6.1), 4.29 (1H, s)	7.12 (2H, d, 8.6), 6.95 (2H, d, 8.6), 6.70 (2H, d, 8.6), 6.64 (2H, d, 8.6)	3.10, 3.02, 2.88, 2.86
14b ($CDCl_3$)	–	5.77 (1H, s), 5.27 (1H, m), 3.96 (1H, d, 5.8)	7.11 (2H, d, 8.4), 6.95 (2H, d, 8.4), 6.65–6.57 (4H, m)	2.90–2.84
16 ($CDCl_3$)	1.60	5.62 (1H, d, 7.4), 5.43 (1H, d, 7.4), 4.79 (1H, d, 7.4), 4.75 (1H, d, 7.4)	8.00 (1H, d, 7.6), 7.71–7.50 (3H, m), 6.82 (2H, d, 8.6), 6.69 (2H, d, 8.6)	–

[a] δ_H in ppm. Coupling pattern and coupling constant (in Hz) are shown in parentheses.
[b] For other signals: **10**: cod signals: 3.66–3.44 (4H, m), 2.45–2.23 (8H, m). **13a**: piperidine: 2.43–1.17. **13b**: PEt_3: 1.80 (6H, m, CH_2), 0.87 (9H, m, CH_3). **12**: 6.21 (CH). **14a**: 7.83 (1H, s, NH), 5.86 (1H, s, CH), 3.18–1.31 (piperidine). **14b**: 5.37 (1H, s), 1.32 (6H, CH_2), 0.88 (9H, CH_3).

3). The compositions (1:1 adducts) were readily determined on the basis of the intensities of the ^{1}H NMR signals for the MY and Cp* ligands (Table 1), and the coordination sites were also readily determined on the basis of the assignments of the aromatic signals shifted to higher field (Fig. 1 and Table 1). It is established that coordination of an aromatic group to a transition metal species in η^6-fashion causes upfield-shifts of the aromatic proton signals [4–6]. As shown in Fig. 1, the signals for the α and β rings are assigned on the basis of the coupling patterns; α ring: three multiplet signals for the *o*-, *m*-, and *p*-hydrogen atoms; β ring: a pair of coupled doublets (δ_H 6.76, 7.91 (d, $J = 7.2$ Hz)). In the case of **5a** · PF_6, the signals assigned to the α ring are shifted to higher field leading to the assignment to the α ring adduct. On the other hand, the ^{1}H NMR spectrum of **5b** · PF_6 contains the doublet pairs shifted to higher field leading to the assignment to the β ring adduct. Thus it is revealed that the major product **5b** · PF_6 results from coordination to the C_6H_4–NMe_2 part (β ring). The assignments have been verified by X-ray crystallography (Fig. 2a and b). A remarkable difference is noted for UV–Vis spectra. The α ring adduct **5a** · PF_6 shows a visible absorption at 504 nm with the intensity comparable to that of **1**, whereas the intensity of the 500 nm absorption observed for **5b** · PF_6 is much weaker that those of **5a** · PF_6 and **1** presumably because of the negligible contribution of the colored, quinoidal form (see **F′** in Scheme 9).

It is notable that the analogous reaction of the protonated form of **1**, [**1**+H] · OTf, inverted the isomer ratio to give **5a** · PF_6 as the dominant product (5:1). These results can be interpreted as follows. The direct reaction with **1** results in coordination to the electron-rich β ring bearing the NMe_2 group. Protonation of **1** occurs at the nitrogen atom attached to the α ring to decrease the electron density of the β ring and, therefore, the $RuCp^{*+}$ fragment should be attached to the more electron-rich α ring in the protonated form ($[\mathbf{1}+H]^+$) to give **5a** · PF_6. Contribution of the quinoidal form ($[\mathbf{1}+H]'^+$ in Scheme 2), which cannot be coordinated in a η^6-fashion, should also promote coordination to the aromatic α ring.

For comparison sake, the NPh_2 derivative of **5** · PF_6 (**5a′** · PF_6) was also prepared. In this case, the adduct of the α ring (**5a′** · PF_6) was obtained as the major product (**5a′** · PF_6:**5b′** · PF_6 = 5:2) even from the non-protonated precursor **1′**, presumably because (i) the lone pair electrons on the NPh_2 part are delocalized over the NAr_3 part to decrease electron density of the α ring (compared to **1**) and (ii) the bulky Ph substituents may hinder approach of the bulky $RuCp^*$ fragment to the β ring. Reaction with [**1′**-H]OTf improved the selectivity for **5a′** · PF_6 (**5a′** · PF_6:**5b′** · PF_6 = 8:1). The adduct of the NPh_2 part was not detected at all.

Preparation of the $RuCl_2$(L) adduct was also attempted but reaction of **1** with Ru(cod)(naphthalene) did not afford the desired η^6-arene complex, (η^6-MY)Ru(cod), as observed for CVL (see below). Because azobenzene without the NMe_2 group gave the 1:1 adduct, (η^6-azobenzene)Ru(cod), as judged by ^{1}H NMR, the failure in the formation of the **1**-adduct should be ascribed to the NMe_2 substituent, which might work as a σ-donor.

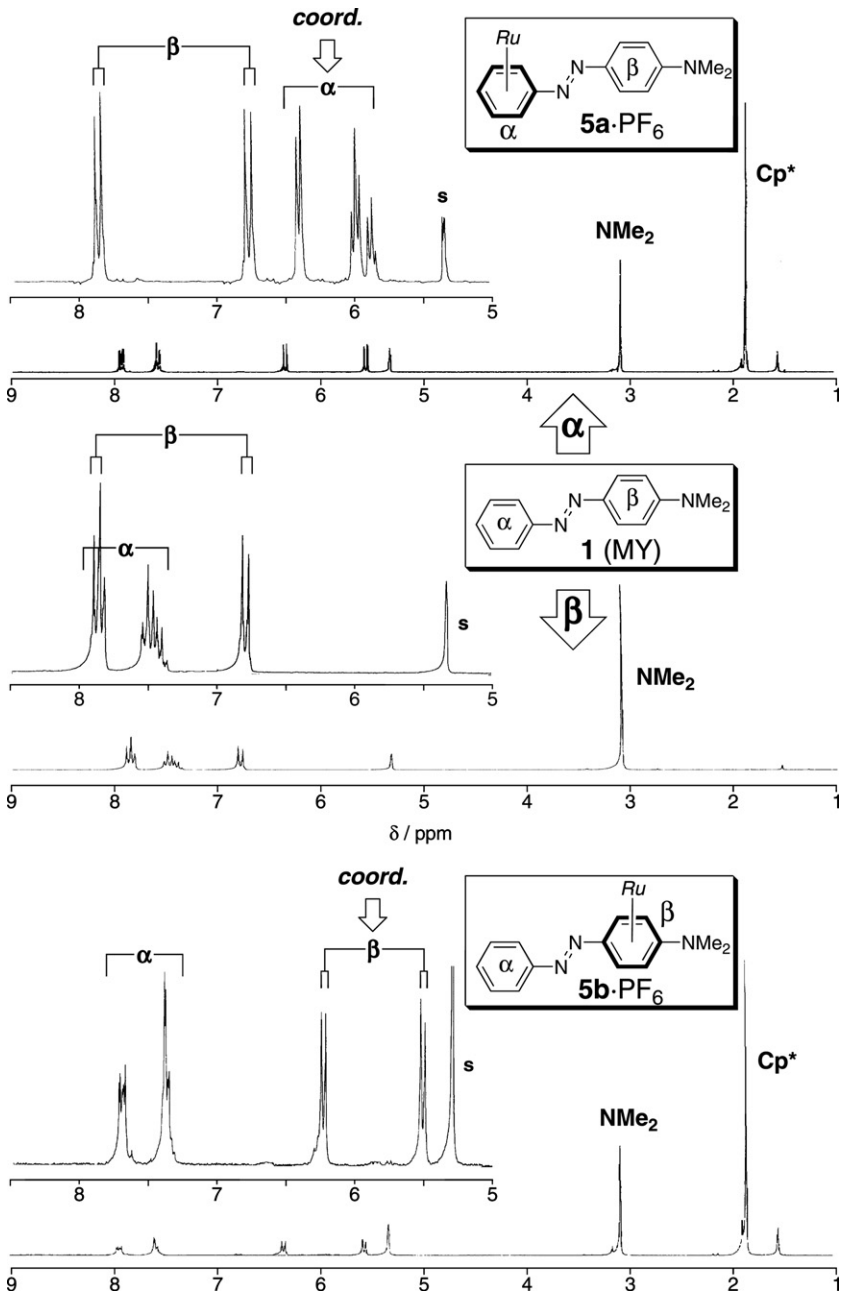

Fig. 1. ^{1}H NMR spectra for **1**, **5a** · PF_6, and **5b** · PF_6 observed in CD_2Cl_2 at 400 MHz (s: residual protio solvent signals; ∗: impurities).

*2.1.1.2. $Cr(CO)_3$ complexes, $[(\eta^6\text{-}MY)Cr(CO)_3]PF_6$ (**6**).* Reaction of **1** with $Cr(CO)_6$ in Bu_2O–THF at 120 °C in a glass autoclave gave an isomeric mixture of the η^6-adduct **6a** and **6b** in a low yield accompanying formation of a large amount of black precipitates which did not show ν(CO) vibration (Scheme 3). Reaction at higher temperature (>170 °C) caused decomposition of the product, and reaction of the protonated precursor [**1**+H]OTf did not afford **6** presumably because of its low solubility in the reaction medium. The two regioisomers **6a**,**b** could not be separated by neither recrystallization nor chromatography but by hands, because the crystal shapes were considerably different (**6a**: needles; **6b**: plates). The two isomers were readily characterized by analyzing the shifted ^{1}H NMR signals for the coordinated arene parts in a manner similar to **5** · PF_6 (Table 1). The presence of the $Cr(CO)_3$ auxiliary was confirmed by the characteristic two strong ν(CO) vibrations and the ^{13}C NMR signals (δ_C 233). Molecular structures of the two isomers were determined by X-ray crystallography (Fig. 2d and e).

2.1.2. Crystal violet lactone complexes

Crystal violet lactone (CVL; **2**) opens the lactone ring under acidic conditions through protonation at the COO moiety to show violet color based on the resonance

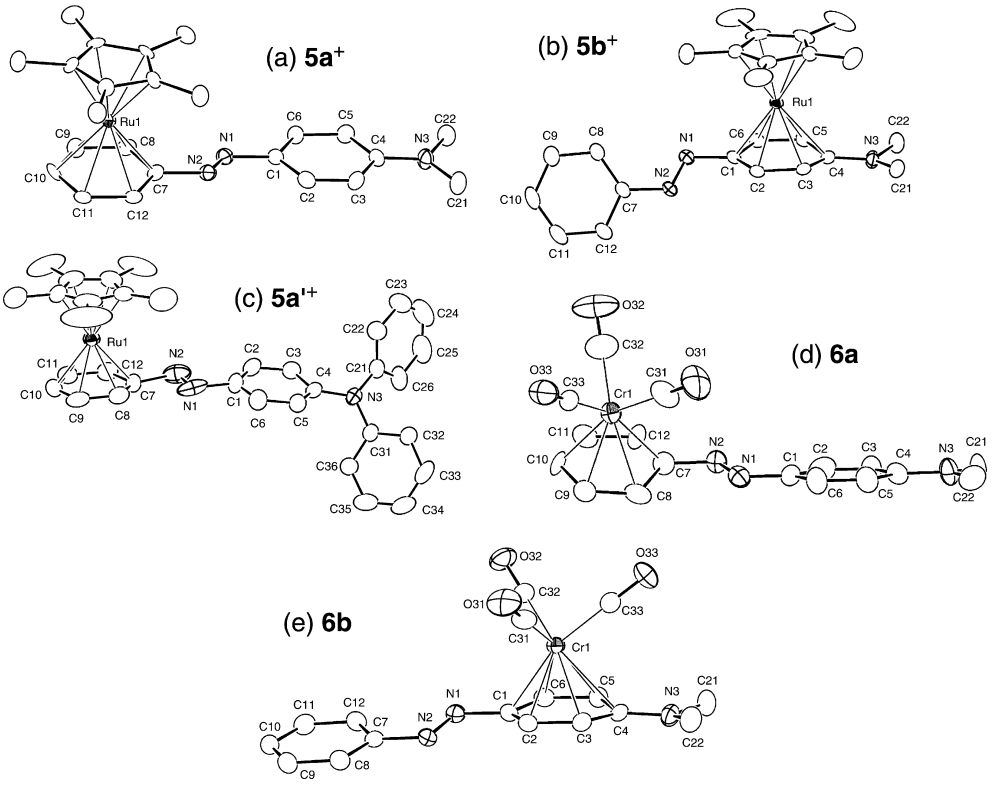

Fig. 2. Molecular structures of the methyl yellow complexes drawn with thermal ellipsoids at the 30% probability level. (a) $\mathbf{5a}^{+}$, (b) $\mathbf{5b}^{+}$, (c) $\mathbf{5a'}^{+}$, (d) **6a**, and (e) **6b**.

structures **C′**, **C″**, etc. (Scheme 2). Synthesis and characterization of the CVL–Ru complexes are described below [9]. We also examined the reaction with $Cr(CO)_6$ but no characterizable product was obtained.

2.1.2.1. Cationic RuCp complexes, $[(\eta^6\text{-CVL})RuCp^*]PF_6$ ($7\cdot PF_6$) and $[(\eta^6\text{-CVL})(RuCp^*)_2](PF_6)_2$ ($\mathbf{8}\cdot(PF_6)_2$) (CVL = crystal violet lactone).* Treatment of **2** with $\mathbf{4}\cdot PF_6$ in CH_2Cl_2 caused immediate color change from

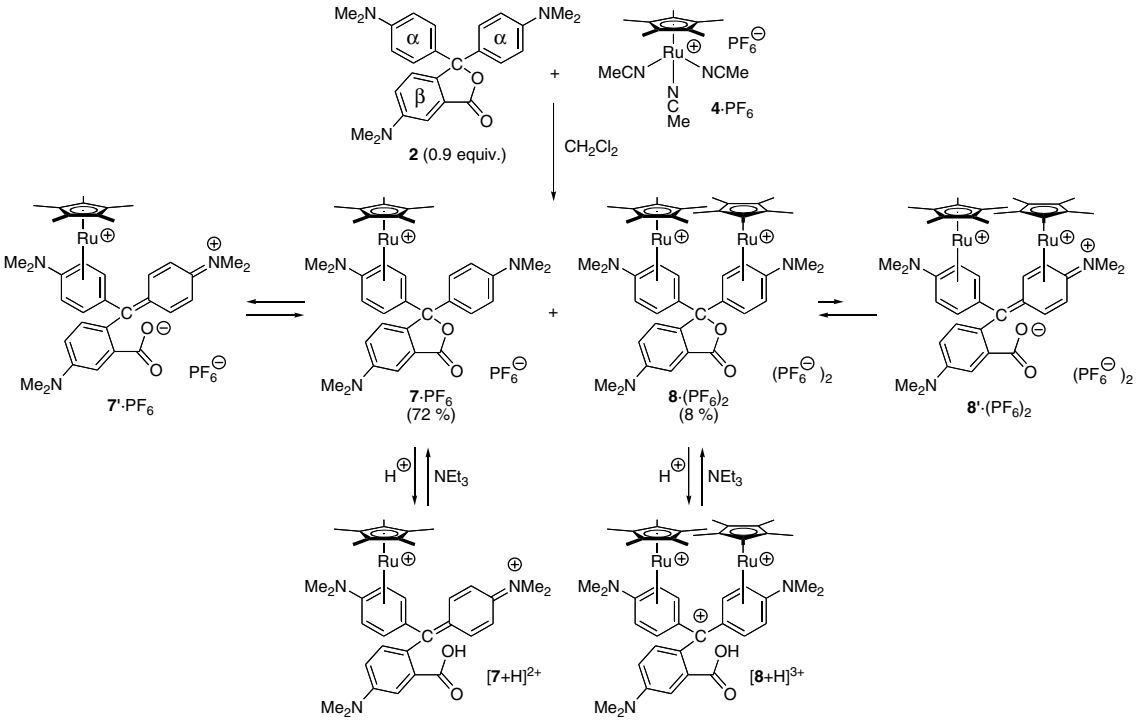

Scheme 4.

yellow to deep blue (Scheme 4). Chromatographic separation (alumina) gave two pale blue products, $\mathbf{7}\cdot PF_6$ (72%) and $\mathbf{8}\cdot(PF_6)_2$ (9%), which were characterized to be mono- and dinuclear adducts, respectively, as described below. The 1:2 adduct $\mathbf{8}\cdot(PF_6)_2$ was obtained as the major product by the 1:2 reaction, while a 1:1 reaction with the protonated CVL ($[\mathbf{2}+H]^+\cdot OTf$) afforded the mononuclear product preferentially ($\mathbf{7}\cdot PF_6/\mathbf{8}(PF_6)_2 = 20{:}1$).

The number of the attached $RuCp^*$ fragments and the coordination site were also readily determined in a manner similar to the MY complexes $\mathbf{5}\cdot PF_6$ (Fig. 3 and Table 1). As shown in Fig. 3a, the pair of two doublet signals for **2** at δ_H 6.62 and 7.13 was assigned to the signals for the α-ring and the remaining aromatic signals to the β-ring. Upon coordination, half of the doublet pair was shifted to higher field (δ_H 5–6), whereas no significant shift was observed for the remaining half and the signals for the β-ring (Fig. 3b). These spectral changes revealed that the $RuCp^*$ fragment was coordinated to one of the two α-rings. In the case of $\mathbf{8}\cdot(PF_6)_2$ (Fig. 3c), the doublet pair was com-

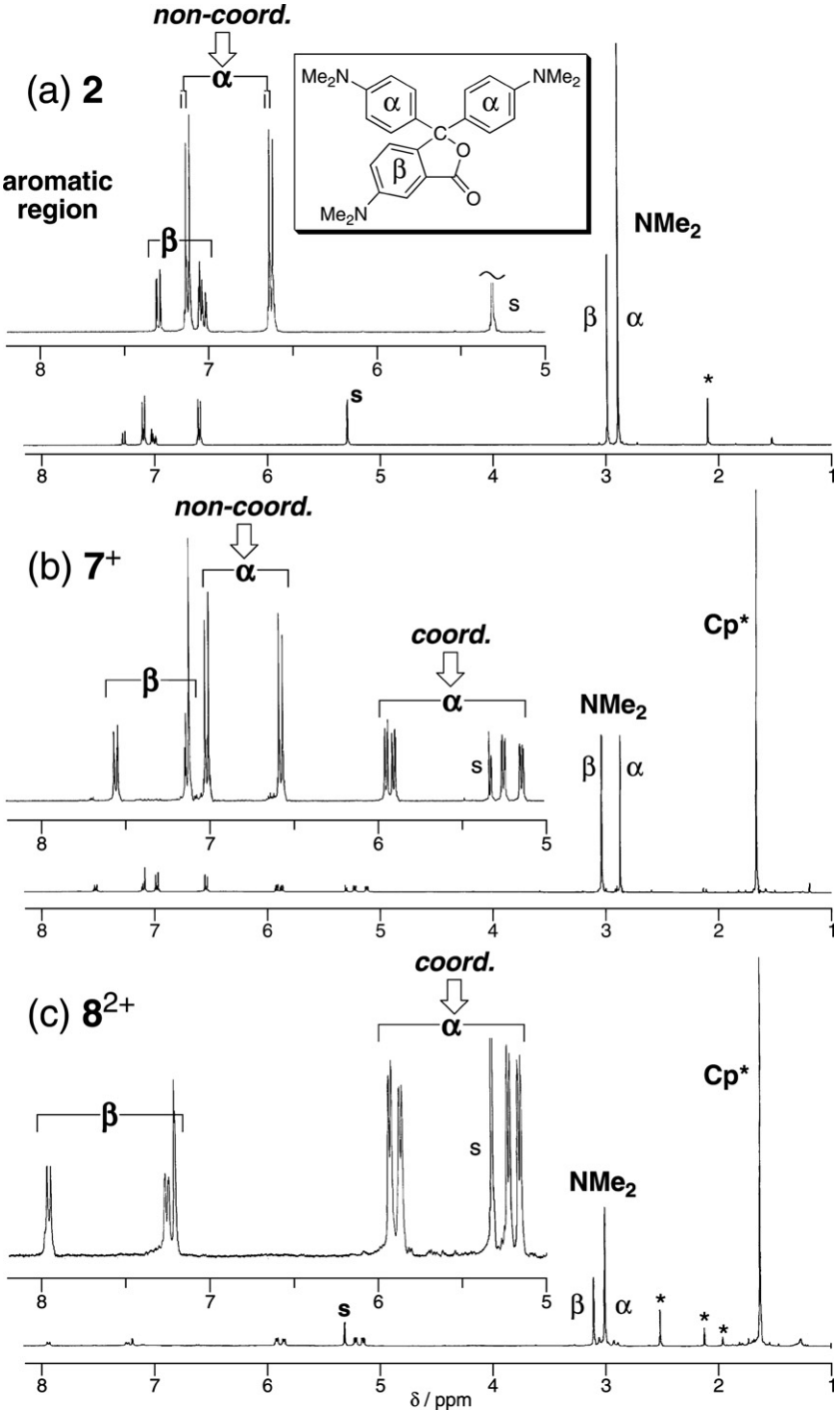

Fig. 3. ^1H NMR spectra for **2** (a), $\mathbf{7}^+$ (b), and $\mathbf{8}^{2+}$ (c) observed in CD_2Cl_2 at 400 MHz (s: residual protio solvent signals; ∗: impurities).

pletely shifted to the higher field, indicating coordination of the $RuCp^*$ fragments to the two α-rings. Coordination of the bulky $RuCp^*$ fragments hinders rotation around the C–(η^6-Ar)Ru axis to cause separation of the α ring signals into two pairs of doublets. Thus the $RuCp^{*+}$ fragment is attached to the more electron-rich α ring in a selective manner as also confirmed by X-ray crystallography (Fig. 4a and b, see below).

The NMR data confirmed the compositions of the adducts $\mathbf{7}\cdot PF_6$ and $\mathbf{8}\cdot(PF_6)_2$ but the structure of the lactone moiety (open or closed) could not be deduced from the NMR data alone. On the other hand, IR spectra of the adducts contained not only the $\nu_{C=O}$ vibrations assignable to the closed lactone group (1759 ($\mathbf{7}\cdot PF_6$), 1775 cm^{-1} ($\mathbf{8}\cdot(PF_6)_2$)) but also weak absorptions assignable to the open carboxylate group (1557 ($\mathbf{7'}\cdot PF_6$), 1565 cm^{-1} ($\mathbf{8'}\cdot(PF_6)_2$)), suggesting formation of both of the closed and open forms. In addition, UV–Vis spectra (see for example, Fig. 5) contained weak absorptions around 600 nm attributable to the open forms $\mathbf{7'}\cdot PF_6$ and $\mathbf{8'}\cdot(PF_6)_2$. These data suggested that the two forms were equilibrated in solutions and, judging from the intensities of the UV–Vis absorptions weaker than those of the protonated open forms, $[\mathbf{7}+H]^{2+}$ and $[\mathbf{8}+H]^{3+}$, the closed forms should be the dominant species in solutions. The equilibrium observed for $\mathbf{7}^+$ and $\mathbf{8}^{2+}$ is in sharp contrast to the non-coordinated CVL (**2**), for which the colored open form is not detected (even by the naked eyes). This difference sounds strange, because attachment of a cationic fragment to the α-ring(s) in **2** should destabilize the open form with the cationic charge on the π-conjugated system coordinated by the cationic $RuCp^*$ fragment(s). The difference could be interpreted in terms of the X-ray structures discussed below.

The solid-state structures of the open forms of $\mathbf{7}\cdot PF_6$ and $\mathbf{8}\cdot(PF_6)_2$ were determined by X-ray crystallography (Fig. 4a and b). For the CVL parts no significant difference is noted when compared with **2** [10]. Molecule $\mathbf{7}^+\cdot PF_6$ sits on a crystallographic mirror plane passing through Ru1, C1, O1, C11 and so on, and the C2–O2 moiety being refined with the occupancy of 0.5 is disordered with respect to the mirror plane. The structures are consistent with the above-mentioned spectroscopic characterization including the number of the attached $RuCp^*$ fragments and the coor-

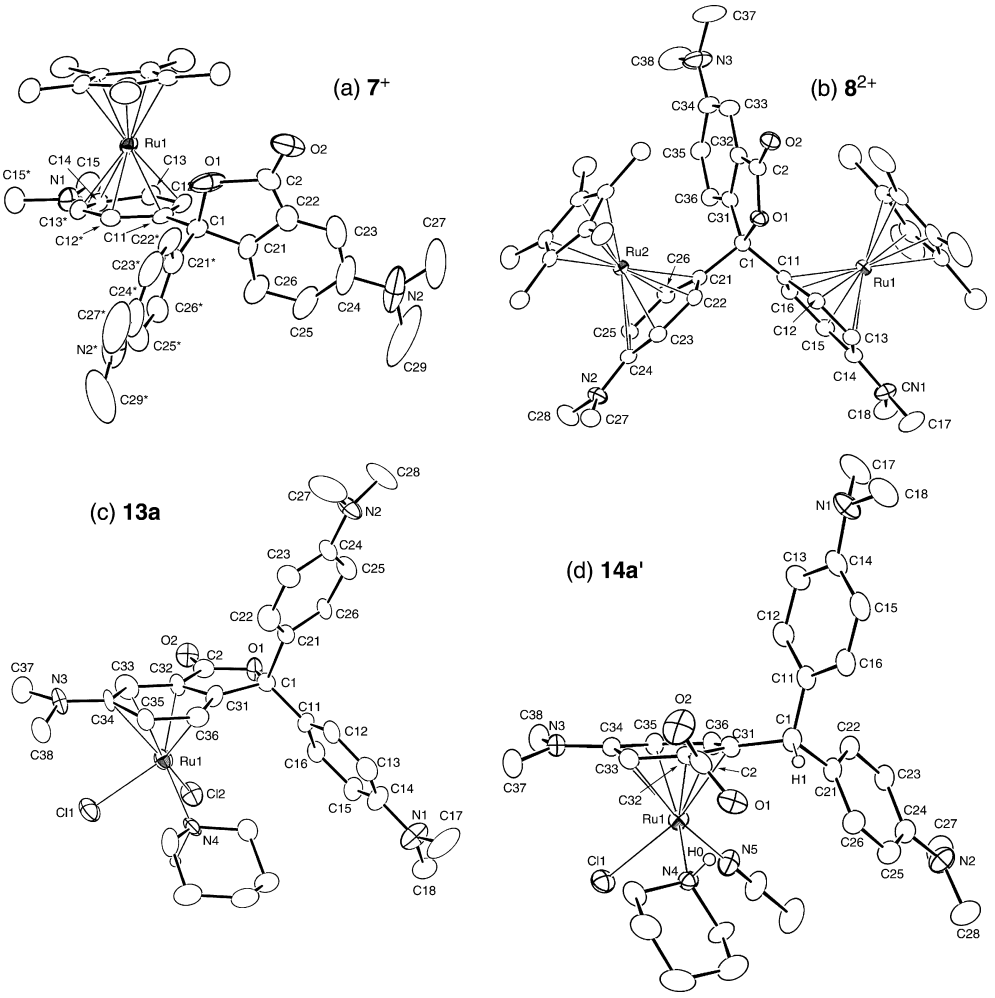

Fig. 4. Molecular structures of the ruthenium complexes derived from crystal violet lactone drawn with thermal ellipsoids at the 30% probability level. (a) $\mathbf{7}^+$ (cationic part), (b) $\mathbf{8}^{2+}$ (cationic part), (c) **13a**, and (d) **14a′**.

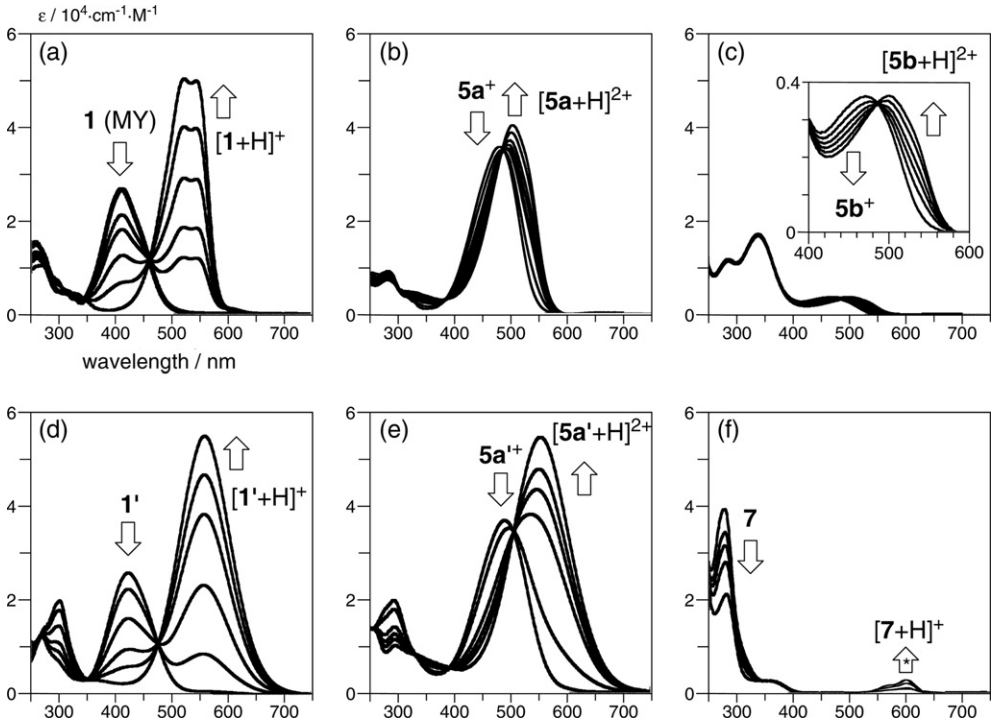

Fig. 5. Addition of acid to pH-indicators and their complexes as monitored by UV-spectroscopy (in CH_2Cl_2; (a)–(e) CH_3SO_3H; (f) CF_3SO_3H). * ($[7+H]^+$): see text.

dination sites (α-ring). One of the key features of $\mathbf{7}\cdot PF_6$ is the coplanar geometry of the Ru1–C11–C1–O1 moiety (dihedral angle = 0°) associated with the close contact between the Ru1 and O1 atoms (3.520(7) Å). The similar feature is noted for $\mathbf{8}\cdot(PF_6)_2$ [Ru1–O1: 3.864(3), Ru2–O1: 3.937(3) Å]. Such short contacts should result from electrostatic, attractive interactions between the cationic ruthenium center and the electronegative lactone oxygen atom(s). The equilibria mentioned above ($\mathbf{7}^+ \leftrightarrow \mathbf{7'}^+$, $\mathbf{8}^{2+} \leftrightarrow \mathbf{8'}^{2+}$; Scheme 4) could be explained on the basis of the electrostatic interaction (Scheme 5), which may facilitate the ring opening and stabilize the resultant negative charge developed on the oxygen atom, although no significant elongation of the C1–O1 bonds (**7**: 1.45(1) Å; **8**: 1.455(4) Å) is observed and the ruthenium centers are coordinatively saturated. Other structural features will be discussed below.

*2.1.2.2. $RuCl_2(L)$ complexes, (η^6-CVL)$RuCl_2(L)$ (**13**).* The $[Cp^*Ru(\eta^6\text{-arene})]^+$ species are stable enough to be fully characterized, as described above, and easy to deal with as the initial synthetic targets. But they are coordinatively saturated and then we sought to prepare a more reactive system, i.e. (η^6-arene)$RuCl_2(L)$. Because, however, preparation of $[(\eta^6\text{-arene})Ru(\mu\text{-Cl})]_2$-type complexes with a functionalized arene molecule has few precedents, synthesis of an $[(\eta^6\text{-arene})Ru(\mu\text{-Cl})]_2$ complex with a pH-indicator, a highly functionalized molecule, is a challenging problem [11].

(η^6-Arene)$RuCl_2(L)$-type complexes can be prepared by treatment of $[(\eta^6\text{-arene})Ru(\mu\text{-Cl})]_2$ complexes with appropriate donors (L) [12]. The precursors, $[(\eta^6\text{-arene})Ru(\mu\text{-Cl})]_2$, have been prepared mainly by two methods: (i) arene-exchange reaction of $[(\eta^6\text{-}p\text{-cymene})Ru(\mu\text{-Cl})]_2$ conducted by heating at the boiling point (or above the melting point) of the arene to be introduced [13]; and (ii) HCl-treatment of (η^6-arene)Ru(η^4-cod), which is obtained by treatment of the arene with (η^6-naphthalene)Ru(η^4-cod) (**9**) or (η^6-cot)Ru(η^4-cod) [14]. We examined these reactions and found that the desired compound could be prepared by method (ii) starting from **9**. Method (i) is not applicable to solid aromatic substances and the reaction at the melting point of CVL causes its decomposition.

Reaction of **2** with **9** in THF in the presence of MeCN followed by separation by chromatography under Ar gave the yellow, air-sensitive product **10**, which was characterized only by ^1H NMR because of its sensitivity to the air (Scheme 6). The 1:1 stoichiometry was confirmed by the intensities of the CVL and cod signals. The coordinated arene ring was readily determined to be the β-ring on the basis of the upfield-shifted aromatic ring signals (Table 1). It is notable that the adduct formation on the β ring contrasts with the addition to the α-ring observed for $\mathbf{7}^+$

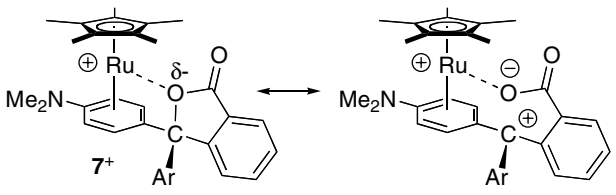

Scheme 5.

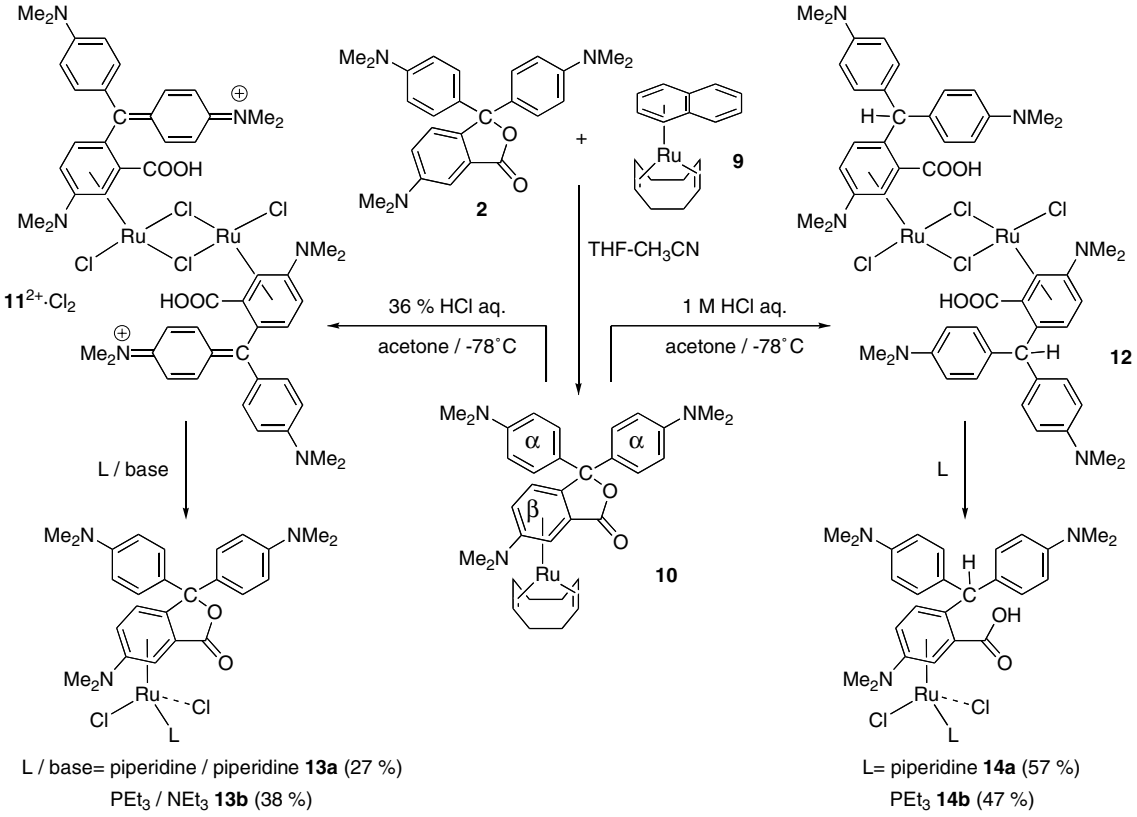

Scheme 6.

and $\mathbf{8}^{2+}$, and the different regiochemistry can be formally interpreted in terms of the difference in the oxidation state. The Ru(0) center in **10** may prefer coordination to the aromatic ring, where back donation is most effective, and, therefore, the β ring bearing the electron-withdrawing carboxyl group should be the preferential reaction site [15].

Subsequent HCl-treatment of **10** gave two different products depending on the concentration of the HCl solution. Addition of 36% HCl aqueous solution diluted with acetone (1:100) caused immediate precipitation of orange solid $\mathbf{11} \cdot Cl_2$, whereas treatment with 1 M HCl aqueous solution diluted with acetone (1:20) gave red product **12** (Scheme 6).

The cationic complex $\mathbf{11} \cdot Cl_2$ was characterized as the dicationic, dimeric, open-protonated form with the Cl bridges but its detailed characterization was hampered by its low solubility in organic solvents and formation of diastereomers. But its ^{1}H NMR spectrum observed in DMSO-d_6 contained signals around δ_H 6.5–4.5 suggesting retention of the (η^6-arene)Ru interaction, and the ESI-MS peaks around $m/z = 1143$ (**11**−Cl) supported the formulation. The resultant green color suggested formation of an open structure, which should be formed by the protonation at the lactone group by excess HCl present in the mixture (Scheme 2). Characterization of the other neutral product **12** will be described below.

Conversion of $\mathbf{11} \cdot Cl_2$ into mononuclear ring-closed products through cleavage of the Ru–Cl–Ru bridging interactions could be effected by a combination of deprotonation and coordination of a 2e-donor. Piperidine, an amine, should achieve both of the functions and, in fact, treatment of $\mathbf{11} \cdot Cl_2$ with piperidine gave the mononuclear adduct **13a** (Scheme 6). Coordination site of the Ru fragment was determined to be the β-ring on the basis of the shifted signals assigned to that part (Table 1), and the appearance of the piperidine signals confirmed its coordination. The closed structure was suggested by the $\nu_{C=O}$ vibration at 1777 cm^{-1} and the lack of $\nu_{C=O}$ vibration for a carboxylate group. Reaction of with $\mathbf{11}^{2+} \cdot Cl_2$ with PEt_3 in the presence of NEt_3 also gave the corresponding adduct **13b**, which showed spectroscopic features similar to those of **13a** (Table 1).

The spectroscopic features of **13a** are consistent with the molecular structure determined by X-ray crystallography (Fig. 4c). The N–H moiety forms hydrogen-bonding interaction with the two chloro ligands.

The red product **12** obtained by treatment of **10** with a diluted HCl solution was also characterized after conversion to the piperidine (**14a**) and PEt_3 adducts (**14b**) because of the low solubility of **12** in common organic solvents and formation of the diastereomers (Scheme 6). The adduct **14** showed four ^{1}H NMR signals in the region where the coordinated η^6-arene signals appeared. Such a data was not consistent with the desired product $\mathbf{11}^{2+}$ (with three η^6-Ar signals) but **14** could not be characterized by the spectroscopic data alone. Attempted crystallization of **14a** from

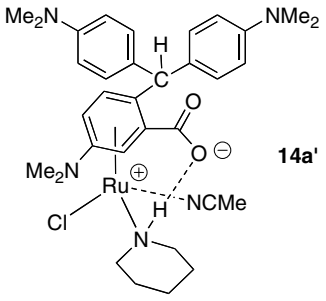

Scheme 7.

acetonitrile gave a small amount of orange red crystals **14a′**, which was subjected to X-ray crystallography. As a result, **14a′** turned out to be the zwitterionic reduced product resulting from Cl-replacement by MeCN (Scheme 7). The most striking feature is that a hydrogen atom is attached to the central carbon atom as confirmed by its hybridization characterized by the sum of the three C–C–C angles (336.5°; cf. **13a**: 360°). On the basis of the structure of **14a′**, complexes **12** and **14** were characterized to be the μ-Cl dimer complex bearing the reduced arene ligand and the donor-coordinated mononuclear complex, respectively. In accord with the structures, the lactone C═O vibration observed for **13** (~1770 cm^{-1}) disappears in **14** and the singlet ^1H NMR signals around δ_H 5.9 (**14**) are assigned to the central H–CAr_3 part. Although the formation mechanism of **14** is not clear, the reduced ligand might be formed via electron transfer to the open trityl cation-type intermediate followed by H-abstraction.

2.1.3. Phenolphthalein–RuCp* complexes

In contrast to CVL, phenolphthalein (PP; **3**) exhibits pink color under basic conditions through deprotonation of the phenolic hydrogen atom (Scheme 2). Compared to the other pH-indicators studied herein, **3** is sparingly soluble in organic solvents to hamper solution chemistry. For example, reaction of **3** with **4** · PF_6 suspended in CH_2Cl_2 in a manner analogous to the synthesis of **7** · PF_6 resulted in a very low conversion and the product could not be isolated from the mixture (Scheme 8). Then we changed the synthetic method from the η^6-coordination (to $\mathbf{4}^+$) to neutralization reaction with a basic precursor, $[Cp^*Ru(\mu\text{-}OMe)]_2$ (**15**). It was expected that the neutralization was so fast as to drive dissolution of **3** in CH_2Cl_2 and finally led to a high conversion. As we expected, treatment of **3** with an equimolar amount of **15** in MeOH gave the neutral 1:1 adduct **16** (Scheme 8) [16]. Although an analytically pure sample could not be obtained, the product was satisfactorily characterized as the α ring adduct on the basis of its ^1H NMR data (Table 1).

Preparation of the corresponding $RuCl_2(L)$ and $Cr(CO)_3$ complexes was hampered by the lack of appropriate basic precursors.

2.2. Molecular structures of the pH-indicator complexes

Of the complexes obtained by the present study, the seven Ru complexes (**7** · PF_6, **8** · $(PF_6)_2$, **13a**, **14a′**, **5a** · PF_6, **5b** · PF_6, and **5a′** · PF_6) and the two Cr complexes (**6a** and **6b**) were characterized by X-ray crystallography. Selected bond lengths are summarized in Tables 2 and 3.

The η^6-coordination of the arene moieties is evident from the M–C distances in the ranges of the bonding interactions (2.1–2.4 Å), and the C–C distances of the coordinated arene parts are slightly longer than those of the non-coordinated arene parts owing to the back donation from the metal centers [15]. The coordination is not always symmetrical, and the complexes are divided into two groups. In the case of the $(\eta^6\text{-}C_6H_xNMe_2)M$ complexes (**5b** · PF_6, **6b**, **7** · PF_6, **8** · $(PF_6)_2$, **13a**, and **14a′**), the differences between the longest and shortest M–Ar distances (*Δ* in Tables 2 and 3) are in the

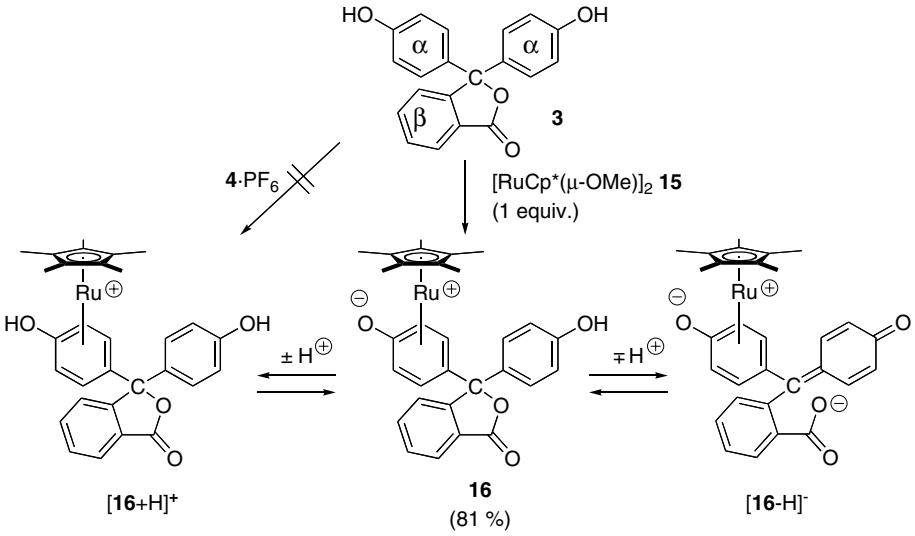

Scheme 8.

Table 2
Selected bond lengths (Å) for the methyl yellow complexes

Complex	**5a** · PF_6	**5b** · PF_6	**5a′** · PF_6	**6a**[a]		**6b**
C1–C2	1.405(9)	1.419(6)	1.40(2)	1.44(2)	1.40(2)	1.384(6)
C1–C6	1.389(8)	1.405(6)	1.35(2)	1.38(2)	1.42(2)	1.420(6)
C2–C3	1.38(1)	1.416(6)	1.38(1)	1.31(2)	1.39(2)	1.417(6)
C3–C4	1.416(9)	1.434(6)	1.38(2)	1.40(2)	1.41(2)	1.439(6)
C4–C5	1.410(9)	1.431(6)	1.37(2)	1.42(2)	1.42(2)	1.436(6)
C5–C6	1.40(1)	1.417(6)	1.39(2)	1.34(2)	1.32(2)	1.412(6)
C7–C8	1.416(9)	1.395(6)	1.34(2)	1.44(2)	1.50(2)	1.393(6)
C7–C12	1.432(8)	1.397(6)	1.45(2)	1.42(2)	1.35(2)	1.380(6)
C8–C9	1.41(1)	1.390(7)	1.43(2)	1.41(2)	1.38(2)	1.369(7)
C9–C10	1.42(1)	1.403(7)	1.38(2)	1.39(2)	1.38(2)	1.376(8)
C10–C11	1.402(9)	1.368(8)	1.39(2)	1.40(2)	1.42(2)	1.389(7)
C11–C12	1.41(1)	1.381(7)	1.38(2)	1.37(2)	1.43(2)	1.379(7)
C1–N1	1.408(9)	1.435(5)	1.55(2)	1.37(2)	1.39(2)	1.429(6)
N1–N2	1.252(7)	1.260(5)	1.13(2)	1.29(2)	1.26(2)	1.253(5)
N2–C7	1.437(9)	1.432(5)	1.60(1)	1.41(2)	1.43(2)	1.430(5)
N3–C4	1.36(1)	1.352(6)	1.42(1)	1.38(2)	1.36(2)	1.333(6)
M–Ar	2.221(6) (C7)	2.211(4) (C1)	2.237(9) (C7)	2.21(1)	2.24(1) (C7)	2.224(5) (C1)
	2.208(5) (C8)	2.220(4) (C2)	2.20(2) (C8)	2.27(2)	2.23(2) (C8)	2.208(5) (C2)
	2.217(6) (C9)	2.231(4) (C3)	2.23(1) (C9)	2.19(2)	2.20(2) (C9)	2.260(5) (C3)
	2.212(7) (C10)	2.374(4) (C4)	2.18(1) (C10)	2.21(2)	2.24(2) (C10)	2.394(4) (C4)
	2.235(6) (C11)	2.235(4) (C5)	2.22(1) (C11)	2.21(2)	2.19(2) (C11)	2.258(4) (C5)
	2.214(5) (C12)	2.193(4) (C6)	2.21(2) (C12)	2.25(1)	2.22(2) (C12)	2.190(4) (C6)
Δ[b]	0.027	0.181	0.057	0.08	0.05	0.204
M–L	2.167–2.205(6) (Cp^*)	2.166–2.187(5) (Cp^*)	2.16–2.208(2) (Cp^*)	1.86(2)	1.83(2) (C31)	1.843(5) (C31)
				1.87(2)	1.78(2) (C32)	1.835(5) (C32)
				1.83(1)	1.83(1) (C33)	1.817(6) (C33)

[a] With two independent molecules.
[b] The difference between the longest and shortest M–C distances.

Table 3
Selected bond lengths (Å) for the crystal violet lactone complexes

Complex	**7** · PF_6	**8** · $(PF_6)_2$		**13a**	**14a′**
M–Ar	2.244(8) (Ru1–C11)	2.235(4) (Ru1–C11)	2.234(4) (Ru1–C21)	2.20(1) (Ru1–C31)	2.206(3) (Ru1–C31)
	2.203(6) (Ru1–C12)	2.213(4) (Ru1–C12)	2.197(4) (Ru1–C22)	2.13(1) (Ru1–C32)	2.191(3) (Ru1–C32)
	2.217(6) (Ru1–C13)	2.225(3) (Ru1–C13)	2.209(3) (Ru1–C23)	2.21(2) (Ru1–C33)	2.201(4) (Ru1–C33)
	2.344(8) (Ru1–C14)	2.360(3) (Ru1–C14)	2.384(3) (Ru1–C24)	2.33(1) (Ru1–C34)	2.360(4) (Ru1–C34)
		2.214(3) (Ru1–C15)	2.236(3) (Ru1–C25)	2.15(2) (Ru1–C35)	2.212(3) (Ru1–C35)
		2.206(4) (Ru1–C16)	2.215(4) (Ru1–C26)	2.12(2) (Ru1–C36)	2.135(3) (Ru1–C36)
Δ[a]	0.141	0.154	0.187	0.21	0.225
C–C	1.418(7) (C11–C12)	1.416(5) (C11–C12)	1.412(5) (C21–C22)	1.41(2) (C31–C32)	1.427(4)(C31–C32)
(η^6–Ar)	1.413(8) (C12–C13)	1.413(5) (C11–C16)	1.402(5) (C21–C26)	1.42(2) (C31–C36)	1.430(6) (C31–C36)
	1.426(7) (C13–C14)	1.413(5) (C12–C13)	1.418(5) (C22–C23)	1.37(2) (C32–C33)	1.431(5) (C32–C33)
		1.424(5) (C13–C14)	1.439(5) (C23–C24)	1.47(2) (C33–C34)	1.430(6) (C33–C34)
		1.418(5) (C14–C15)	1.418(5) (C24–C25)	1.42(2) (C34–C35)	1.420(5) (C34–C35)
		1.418(5) (C15–C16)	1.410(5) (C25–C26)	1.41(2) (C35–C36)	1.415(5) (C35–C36)
C–C (Ar)	1.37–1.40(2)	1.382–1.419(6)		1.37–1.47(2)	1.375–1.431(6)
N–C	1.35(1) (N1–C14)	1.355(5) (N1–C14)	1.357(5) (N2–C24)	1.36(2) (N3–C34)	1.360(5) (N3–C34)
	1.40(1) (N2–C24)	1.373(6) (N3–C34)		1.41(2) (N1–C14)	1.412(5) (N1–C14)
				1.42(2) (N2–C24)	1.380(5) (N2–C24)
M–L	2.161–2.201(8)	2.163–2.200 (5)	2.167–2.2068(4)	2.408(4) (Ru1–Cl1)	2.4223(9) (Ru1–Cl1)
	(Ru1–Cp^*)	(Ru1–Cp^*)	(Ru2–Cp^*)	2.418(4) (Ru1–Cl2)	2.160(9) (Ru1–N4)
				2.12(1) (Ru1–N4)	2.070(3) (Ru1–N5)

[a] The difference between the longest and shortest M–C distances.

range of 0.14–0.23 Å, and the distances from the metal center to the carbon atom attached to the NMe_2 group are always longer than the other M–C distances. The shortest distances for the η^6-$C_6H_5NMe_2$ and η^6-C_6H_4(COO)-(NMe_2) groups are found for the carbon atoms *p* and *m* with respect to the NMe_2 group, respectively. The distortion should arise from the π-donation from the NMe_2 group leading to the η^5-iminocyclohexadienyl structure **D′**

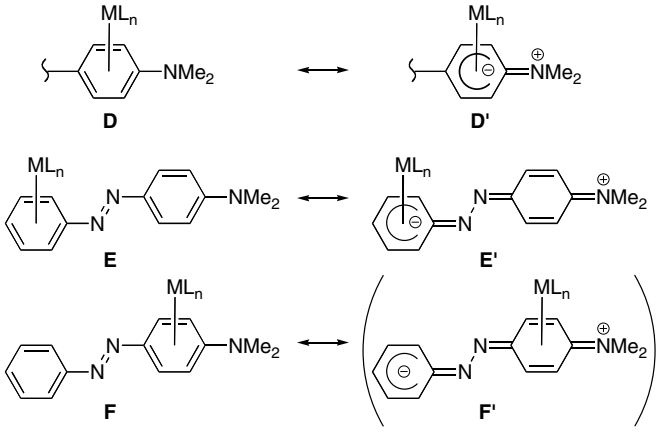

Scheme 9.

(Scheme 9). In the case of the (η^6-C_6H_x–N=N)M complexes (**5a** · PF_6, **5a′** · PF_6, and **6a**), the differences in the M–C distances are less than 0.08 Å and no systematic distortion is found indicating that the electronic effect of the azo group is not significant.

A notable feature observed for the MY complexes is the orientation of the central C–N=N–C moieties. The MY moiety in the β ring adduct **5b** is distorted from a planar structure as indicated by the *s-trans* C–C–N1–N2 and N1–N2–C–C dihedral angles: **5b** · PF_6: 148.3(4)°, 148.0(4)°; cf. **5a** · PF_6: 171.5(5)°, 174.1(5)°, **5a′** · PF_6: 178(1)°, 174(1)°; **6a**: 165(1)°, 176(1)°/166(1)°, 179(1)° (with two independent molecules); **6b**: 173.8(6)°, 165.7(4)°. In the case of the α ring adducts, the planar structure should be stabilized by the quinoidal form **E′**. On the other hand, in the case of the β ring adduct, contribution of the quinoidal form **F′** is negligible because of the quinoid part (a 4e-donor) leading to a 16e configuration. The conformation of the Cr complex **6b** appears to be determined by intermolecular π–π stacking of the α rings.

2.3. Protonation behavior of the pH-indicator complexes

The changes caused by protonation were monitored by ^{1}H NMR and UV–Vis spectroscopy. For accurate comparison with the parent compounds we attempted determination of the pK_a values for the pH indicator complexes on the basis of the titration curves. But the insolubility of the metal complexes in aqueous media hampered the attempts, and the measurements were made in organic solvents. In general, owing to the attachment of the Lewis acidic metal fragments use of a stronger acid is needed for the protonation of the metal complexes. For example, CVL (**2**) can be readily protonated by CH_3COOH, while the mono- (**7** · PF_6) and di-cationic species (**8** · $(PF_6)_2$) are not protonated by CH_3COOH but by CF_3COOH and CF_3SO_3H, respectively.

Protonation behavior of the MY–Ru complexes **5a**,**b** · PF_6 and **5a′** · PF_6 was studied in detail by means of ^{1}H NMR and UV–Vis spectroscopy in CH_2Cl_2/CD_2Cl_2. Addition of CH_3SO_3H to the α ring adduct **5a** · PF_6 caused broadening of the ^{1}H NMR spectrum suggesting occurrence of a fluxional process, while protonation of the NPh_2 derivative **5a′** · PF_6 brought about separation of the doublet pair for the *p*-N_2-C_6H_4-NPh_2 part into two doublet pairs indicating desymmetrization of the *p*-phenylene ring signals. Protonation of the β ring adduct **5b** · PF_6 caused shifts of the signals to lower field. Although the protonation site cannot be determined by the data obtained so far, it is thought that the attachment of the cationic $RuCp^*$ fragment destabilizes some of the possible resonance structures (**H′** for **5a** · PF_6/**5a′** · PF_6 and **I′** for **5b** · PF_6) leading to preferential protonation (*a* for α ring adducts (**5a** · PF_6/**5a′** · PF_6) and *b′* for β ring adduct (**5b** · PF_6)). Thus, for the α ring adducts, the quinoidal form **G′** hinders free rotation around the N–$C_6H_4NR_2$ bond to lead to the desymmetrization, and the fluxional process should be related to the rotation of the =N–C single bond (see Scheme 10).

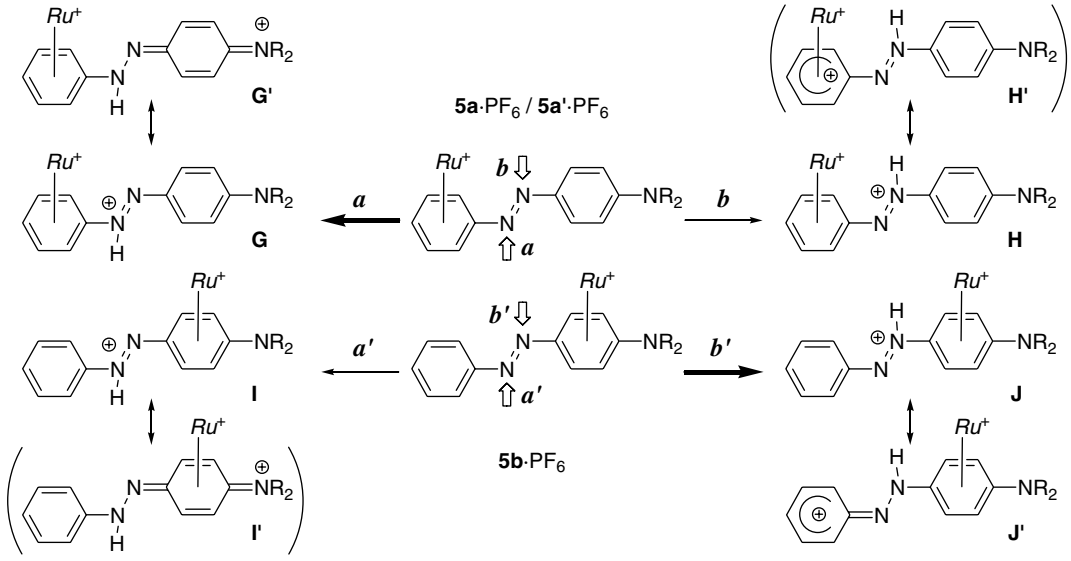

Scheme 10.

The changes of the absorptions brought about by addition of CH_3SO_3H are monitored by UV–Vis spectroscopy and shown in Fig. 5. The parent compounds **1** and **1′** show typical chromic behavior with the substantial separations of the absorption maxima for the two colored forms (**1**: >110 nm; **1′**: 136 nm). The $RuCp^*$ adducts also show smooth spectral change with isosbestic points but the separations of the absorption maxima for the two colored form bare smaller than those of the parent compounds (**5a** · PF_6: 24 nm; **5b** · PF_6: 30 nm; **5a′** · PF_6: 64 nm). Addition of an excess amount of the acid leads to saturated spectra, which can be regarded as the spectra for the protonated forms. On the basis of the intensities of the non-protonated and protonated forms the equilibrium constants for the protonation equilibrium can be calculated as shown in Scheme 11. *K* for **5b** · PF_6 cannot be estimated, because absorption maxima of the two species are too close to be separated. Coordination to the $RuCp^{*+}$ fragment causes a decrease of the *K* values by the order of 10^{-1}–10^{-2} owing to the decreased basicity of MV. The MV–Cr complexes **6a**,**b** decomposed upon acidification.

Protonation of the $[(\eta^6\text{-CVL})RuCp^*]^+$ complexes, **7** · PF_6 and **8** · $(PF_6)_2$, with CF_3COOH or CF_3SO_3H in CD_2Cl_2 causes down field shifts of the signals assigned to the non-coordinated α ring and the β ring; $[\mathbf{7}+H]^{2+}$: δ_H ~5.2, ~5.9 (2H × 2, coordinated α ring) 7.5–8.0 (7H, m, β and non-coordinated α rings); $[\mathbf{8}+H]^{3+}$: δ_H ~5.4, ~5.9 (2H × 2, coordinated α ring) 8.35 (2H, s), 8.48 (1H, s, β ring), while those assigned to the coordinated α ring remained virtually unaffected. This result may be interpreted in terms of the resonance structures of the protonated forms, $[\mathbf{7}+H]^{2+}$ and $[\mathbf{8}+H]^{3+}$ (Scheme 4), where the electronic structures of the coordinated arene parts are little affected. Addition of NEt_3 to $[\mathbf{7}+H]^{2+}$ and $[\mathbf{8}+H]^{3+}$, regenerated $\mathbf{7}^+$ and $\mathbf{8}^{2+}$, respectively, indicating reversibility of the protonation processes. Because NMR provides information concerning the equilibrated mixture of the protonated and non-protonated forms, which are interconverted at a rate faster than the NMR timescale, the protonation was monitored by UV–Vis spectroscopy. Complexes $\mathbf{7}^+$ and $\mathbf{8}^{2+}$, show the UV–Vis bands around 270 nm, which are assigned to the π–π* transition of the closed structure. Upon addition of CF_3SO_3H, the intensity of the absorption decreased and finally disappeared indicating that acidification of $\mathbf{7}^+$ and $\mathbf{8}^{2+}$ containing the closed forms as the major species caused the ring opening of the CVL moiety

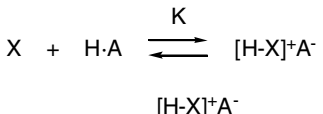

X	K
5a$^+$	4.1 x 10^2
5b$^+$	- [a]
5a'$^{+}$	3.1 x 10
1	1.9 x 10^4
1'	4.0 x 10^2

[a] see text.

Scheme 11.

in a manner similar to the parent CVL molecule (Scheme 2). Acidification caused appearance of the absorption at 605 nm. Because, however, (1) the intensity was variable and (2) it was very similar to that of CVL, we could not eliminate the possibility of partial decomposition under the acidic conditions. We have no evidence for formation of the diprotonated forms. Similar behavior was noted for the $RuCl_2(L)$ adducts **13**. For example, protonation of the PEt_3 complex **13b** with CH_3SO_3H in CD_3OD + $CDCl_3$ (2:1) caused (1) a significant change of the ^1H NMR spectrum, (2) disappearance of the band at 270 nm assignable the π–π* transition, and (3) appearance of the band at 602 nm of variable intensity.

The PP–$RuCp^{*+}$ complex **16** undergoes reversible deprotonation-protonation upon treatment with NaOH and CH_3COOH, respectively, as revealed by the UV-change (**16**: λ_{max} 310 nm ($\varepsilon = 1.9 \times 10^3\ M^{-1}\ cm^{-1}$) → $[\mathbf{16}+H]^+$: 325 nm ($\varepsilon = 2.0 \times 10^3\ M^{-1}\ cm^{-1}$), 557 nm ($\varepsilon = 5.5 \times 10^2\ M^{-1}\ cm^{-1}$)) and ^1H NMR monitoring (Scheme 8).

3. Conclusions

A series of ruthenium and chromium complexes bearing pH indicators as the η^6-arene ligand, $(\eta^6\text{-X})(ML_n)_y$ [X = methyl yellow (**1**), crystal violet lactone (**2**), phenolphthalein (**3**); $ML_n = RuCp^{*+}$, $RuCl_2(L)$, $Cr(CO)_3$; $y = 1, 2$] is prepared and characterized by spectroscopic and crystallographic methods. Of the plural arene rings in the indicator molecules, a specific arene ring can be successfully coordinated to the metal center in a selective manner under appropriate conditions (i.e. use of the metal precursors of different oxidation states and reaction with the non-protonated and protonated pH indicator). The obtained indicator complexes show halochromic behavior depending on pH as observed for the parent molecules. Although most of the obtained complexes are insoluble in water and thus cannot be used as usual pH indicators, the transition pH ranges measured in organic solvents are shifted to the more acidic side compared to the parent indicator molecules because of the attachment of the electron-withdrawing metal fragments, which lower the basicity of the attached pH indicator moieties.

4. Experimental

4.1. General methods

All manipulations were carried out under an inert atmosphere by using standard Schlenk tube techniques. THF, ether (Na–K alloy), CH_2Cl_2, acetone, CH_3CN (P_2O_5), and MeOH ($Mg(OMe)_2$) were treated with appropriate drying agents, distilled, and stored under argon. ^1H, ^{13}C and ^{31}P NMR spectra were recorded on Bruker AC-200 (^1H, 200 MHz; ^{31}P, 81 MHz) and JEOL EX-400 spectrometers (^{31}P, 162 MHz; ^{13}C, 100 MHz). Solvents for NMR measurements containing 0.5% TMS were dried over molecular sieves, degassed, distilled under reduced pres-

sure, and stored under Ar. IR spectra (KBr pellets) were obtained on a JASCO FT/IR 5300 spectrometer. ESI- and FD-mass spectra were recorded on a ThermoQuest Finnigan LCQ Duo and JEOL JMS-700 mass spectrometer, respectively. UV–Vis spectra were obtained with a JASCO V570 spectrophotometer. Compounds **1′** [17], **4** · PF_6 [8] and **9** [18], **15** [19] were prepared according to the published method. Other chemicals were purchased and used as received.

4.2. Preparation of *5a,b* · PF_6

*From **1***: A mixture of **1** (135 mg, 0.602 mmol) and **4** · PF_6 (287 mg, 0.568 mmol) dissolved in CH_2Cl_2 (20 mL) was stirred for 30 min at ambient temperature. The yellow solution gradually turned into red. After removal of the volatiles under reduced pressure the residue was subjected to alumina column chromatography. The orange band eluted with CH_2Cl_2 was collected and crystallized from CH_2Cl_2–ether to give orange crystals (245 mg, 0.404 mmol, 71%), which turned out to be a 1:5 mixture of **5a** · PF_6 and **5b** · PF_6. *From [**1**-H]OTf*: (**1**-H)OTf was prepared by treatment of **1** (226 mg, 1.01 mmol) with TfOH (100 μL, 1.13 mmol) in ether. After cooling the mixture overnight at −30 °C the supernatant solution was removed via a pipette and the residue [(**1**-H)OTf] was dissolved in CH_2Cl_2 (5 mL). To the CH_2Cl_2 solution was added dropwise **4** · PF_6 (293 mg, 0.58 mmol) dissolved in CH_2Cl_2 (5 mL) via a cannula. The mixture was stirred for 1 h and passed through a Celite plug. After removal of the volatiles under reduced pressure the residue was subjected to alumina column chromatography. Compound **1** (yellow band) was first eluted with CH_2Cl_2 and elution with CH_3CN gave orange crystals **5** · PF_6 (190 mg, 0.31 mmol, 54% yield; **5a** · PF_6:**5b** · PF_6 = 5:1). The two regioisomers were separated by recrystallization from CH_2Cl_2–ether. **5a**: δ_C (CD_2Cl_2) 153.9, 142.8, 125.8, 111.3 (Ar), 113.9, 87.1, 81.1 (η^6-Ar), 97.3 (C_5Me_5), 39.8 (NMe_2), 10.2 (C_5Me_5). IR: 1600 (ν_{NN}), 838 (PF_6). ESI-MS: 463 (**5** · PF_6). UV (CH_2Cl_2): λ_{max}/nm ($\varepsilon/M^{-1}\,cm^{-1}$) 480 ($3.6\times10^4$). Anal. Calc. for $C_{24.5}H_{31}N_3F_6PClRu$ [**5a** · PF_6 · $(CH_2Cl_2)_{1/2}$]: C, 45.34; H, 4.81; N, 6.47. Found: C, 44.88; H, 4.96; N, 6.41%. **5b** · PF_6: δ_C (CD_2Cl_2) 151.7, 132.2, 129.1, 122.6 (Ar), 127.4, 108.1 (η^6-Ar), 95.5 (C_5Me_5), 81.2, 69.7 (η^6-Ar), 39.6 (NMe_2), 10.4 (C_5Me_5). IR (KBr) 1562 (ν_{NN}), 837 cm^{-1} (PF_6). ESI-MS: 463 (**5** · PF_6). UV (CH_2Cl_2): λ_{max}/nm ($\varepsilon/M^{-1}\,cm^{-1}$) 337 ($1.8\times10^4$), 470 ($3.7\times10^3$). Anal. Calc. for $C_{24}H_{30}N_3F_6PRu$: C, 47.52; H, 4.99; N, 6.93. Found: C, 47.10; H, 5.28; N, 6.60%.

4.3. Preparation of *5a′* · PF_6

To an ethereal solution of **1′** (140 mg, 0.40 mmol) was added CF_3SO_3H (20 μL, 0.22 mmol). The resultant mixture was stored in a refrigerator (−20 °C) overnight and the supernatant was removed via a pipette. The obtained solid was dried in vacuo and dissolved in CH_2Cl_2. To the resultant solution was added **4** · PF_6 (182 mg, 0.36 mmol) dissolved in CH_2Cl_2 via a cannula over 15 min. After the mixture was stirred overnight, the volatiles were removed under reduced pressure. The residue was subjected to column chromatography (alumina). The unreacted **1′** was eluted with CH_2Cl_2, and elution with CH_3CN gave a red band, crystallization of which from CH_2Cl_2–ether gave **5a′** · PF_6 as yellow crystals (129 mg, 0.176 mmol, 80% yield based on CF_3SO_3H). δ_C (CD_2Cl_2) 152.6, 145.6, 139.5, 129.5, 126.2, 124.9, 119.1, 113.1 (Ar), 97.6 (C_5Me_5), 87.4, 87.2, 82.0 (η^6-Ar), 10.2 (C_5Me_5). IR (KBr) 1588 (ν_{NN}), 839 cm^{-1} (PF_6). ESI-MS: 587 (**5a′** · PF_6). UV (CH_2Cl_2): λ_{max}/nm ($\varepsilon/M^{-1}\,cm^{-1}$) 491 ($2.7\times10^4$). Anal. Calc. for $C_{34.5}H_{35}N_3F_6PClRu$ (**5a′** · PF_6 · $(CH_2Cl_2)_{0.5}$): C, 53.60; H, 4.56; N, 5.43. Found: C, 53.74; H, 4.84; N, 5.33%.

4.4. Preparation of *6a,b*

$Cr(CO)_6$ (885 mg, 4.02 mmol) and **1** (1.11 g, 4.92 mmol) were charged in a glass autoclave. After addition of Bu_2O–THF (10:1, 15 mL) the closed autoclave was heated for 10 h at 120 °C. After removal of the volatiles under reduced pressure the residue was extracted with THF and passed through a Celite plug. The filtrate was evaporated and separated by an alumina column chromatography. Elution with hexane–Et_2O (1:1) gave red crystals composed of **6a** and **6b** (132 mg, 0.42 mmol, 10% yield), which were separated manually. **6a** + **6b**: FD-MS: 316 (**6**). Anal. Calc. for $C_{17}H_{15}N_3O_3Cr$: C, 56.51; H, 4.18; N, 11.63. Found: C, 56.18; H, 4.32; N, 11.36%. **6a**: δ_C (acetone-d_6) 233.8 (CO), 154.3, 137.9, 126.1, 112.3 (Ar), 124.8, 94.3, 94.1, 90.3 (η^6-Ar), 40.3 (NMe_2). IR: 1967, 1870 cm^{-1} (ν_{CO}). **6b**: δ_C (acetone-d_6) 234.0 (CO), 152.7, 131.9, 130.0, 123.2 (Ar), 115.1, 112.3, 94.5, 74.9 (η^6-Ar), 40.1 (NMe_2). IR (KBr) 1942, 1876 cm^{-1} (ν_{CO}).

4.5. Preparation of *7* · PF_6 *and* *8* · $(PF_6)_2$

A mixture of **2** (206 mg, 0.498 mmol) and **4** · PF_6 (213 mg, 0.422 mmol) dissolved in CH_2Cl_2 (5 mL) was stirred for 2 h at ambient temperature. After removal of the volatiles under reduced pressure the residue was subjected to alumina column chromatography. Elution with CH_2Cl_2–CH_3CN (8:1) gave the recovered **2** followed by **7** · PF_6 as a blue band. Further elusion with CH_3CN gave **8** · $(PF_6)_2$ as a blue band. The solvents were evaporated and crystallization of the solids gave $\mathbf{7}^+$ · PF_6 (242 mg, 0.303 mmol, 72% yield, pale blue crystals) and **8** · $(PF_6)_2$ (43 mg, 0.037 mmol, 9% yield, pale blue crystals). **7** · PF_6: δ_C (CD_3CN) 169.6 (C═O), 151.9, 150.4, 137.4, 126.5, 124.5, 119.1, 111.8, 106.2 (Ar + quart. C), 95.3 (C_5Me_5), 87.7, 83.6, 82.1, 67.6, 67.5 (η^6-Ar), 40.4, 40.1, 39.7 (NMe_2), 10.6 (C_5Me_5). IR 1775 ($\nu_{C=O}$), 1622, 1565, 1517, 1444, 1365, 839 (ν_{PF}) cm^{-1}. ESI-MS: 652 (**7**). λ_{max}/nm ($\varepsilon/M^{-1}\,cm^{-1}$ in CH_2Cl_2) 275 (1.53×10^4), 349 (1.25×10^3). Anal. Calc. for $C_{36}H_{44}O_2N_3F_6PRu$: C, 54.23; H, 5.48; N,

5.12. Found: C, 54.27; H, 5.57; N, 5.27%. **8** · $(PF_6)_2$: δ_C (CD_3CN) 168.3 (C═O), 152.7, 128.2, 126.5, 125.3, 119.4, 106.7, 102.6 (Ar), 95.4 (C_5Me_5), 81.2, 81.0, 67.9, 67.6 (η^6-Ar), 40.4, 39.6 (NMe_2), 10.6 (C_5Me_5). IR: 1775 ($\nu_{C=O}$), 1622, 1565, 1517, 1444, 1365, 839 (ν_{PF}) cm^{-1}. ESI-MS: 1033 (**8**). λ_{max}/nm ($\varepsilon/M^{-1}\,cm^{-1}$ in CH_2Cl_2) 277 (2.7×10^4). Anal. Calc. for $C_{46}H_{59}O_2N_3F_{12}P_2Ru_2$: C, 46.48; H, 5.02; N, 3.54. Found: C, 46.89; H, 5.05; N, 3.57%.

4.6. Preparation of *10*

A mixture of **2** (584 mg, 1.41 mmol) and **9** (568 mg, 1.68 mmol) were dissolved in THF (30 mL)–CH_3CN (0.2 mL) and stirred for 2 days at room temperature. The resultant mixture was concentrated to ca. 15 mL under reduced pressure and passed through an alumina plug. The volatiles were removed under reduced pressure and the obtained residue was subjected to alumina column chromatography under argon. The liberated naphthalene and the remaining **9** were first eluted with toluene and then the product **10** was eluted with toluene–THF (25:1). Compound **10** (499 mg, 0.799 mmol, 47% yield) was obtained as yellow solid after evaporation of the solvent. Because **10** was very sensitive to the air, it was characterized only by ^1H NMR and used without further purification.

4.7. Preparation of *11*

Dropwise addition of 36% aq. HCl (diluted with acetone: 1/100) to an acetone solution (10 mL) of crude **10** (155 mg, 0.248 mmol) cooled at −78 °C immediately caused precipitation of orange solid. The mixture was stirred for 6 h at −78 °C. Then the supernatant solution was removed via a pipette, and the residue was washed with pentane and dried under reduced pressure to afford crude $\mathbf{11}^{2+} \cdot Cl_2$ (153 mg. 0.122 mmol, quantitative yield) as orange solid, which was used without further purification. $\mathbf{11}^{2+} \cdot Cl_2$: IR: 1781, 1577, 1509, 1467 cm^{-1}. ESI-MS: 1143 (**11**−Cl).

4.8. Preparation of *12*

Addition of 1 M aq. HCl (diluted with acetone: 1/20; 4 equivalents) to an acetone solution (10 mL) of crude **10** (164 mg, 0.263 mmol) cooled at −78 °C caused color changes from yellow to green and finally to orange. During further stirring for 30 min at room temperature red solid precipitated out of the solution. The volatiles were removed under reduced pressure and the resultant residue was washed with acetone and pentane to leave red solid **12** (quantitative yield), which was used without further purification. **12**: ESI-MS: 1145 (**12**−Cl).

4.9. Preparation of *13a*

To crude $\mathbf{11}^{2+} \cdot Cl_2$ (138 mg. 0.110 mmol) and piperidine (40 μL, 0.40 mmol) was added CH_2Cl_2 (8 mL) and the resultant mixture was stirred for 1 h. The volatiles were removed under reduced pressure and the residue was separated by silica gel column chromatography eluted with CH_2Cl_2–MeOH (20:1) to give **13a** (42 mg, 0.062 mmol, 27% yield) as red-brown powders. **13a**: IR: 1777 (ν_{CO}), 1611, 1562, 1520, 1355 cm^{-1}. ESI-MS: 637 (**13a**−Cl), 552 (**13a**−Cl−L). λ_{max}/nm ($\varepsilon/M^{-1}\,cm^{-1}$ in CH_2Cl_2) 272 (2.1×10^4). Anal. Calc. for $C_{31.5}H_{41}N_4O_2Cl_3Ru$ (**13a** · $(CH_2Cl_2)_{0.5}$): C, 52.91; H, 5.78; N, 7.83. Found: C, 52.41; H, 5.69; N, 7.52%.

4.10. Preparation of *13b*

To a CH_2Cl_2 suspension (8 mL) of crude $\mathbf{11}^{2+} \cdot Cl_2$ (181 mg, 0.144 mmol) prepared as described above were added PEt_3 (40 μL, 0.27 mmol) and NEt_3 (40 μL, 0.29 mmol), and the mixture was stirred for 1 h. The color of the mixture turned from red to yellow green. Separation as described for **13a** gave **13b** (77 mg, 0.011 mmol, 38% yield) as red-brown powders. **13b**: ^{31}P NMR ($CDCl_3$/H_3PO_4) δ_P 11.6. IR: 1771 (ν_{CO}), 1612, 1569, 1519 cm^{-1}. ESI-MS: 670 (**13b**−Cl). UV (MeOH–CH_2Cl_2 = 9:1): λ_{max}/nm ($\varepsilon/M^{-1}\,cm^{-1}$) 270 ($2.7 \times 10^4$). Anal. Calc. for $C_{32.5}H_{45}N_3O_2Cl_3PRu$ (**13b** · $(CH_2Cl_2)_{0.5}$): C, 52.18; H, 6.06; N, 5.62. Found: C, 52.45; H, 6.28; N, 5.96%.

4.11. Preparation of *14a*

To crude **12** (88 mg, 0.0746 mmol) were added CH_2Cl_2 (8 mL) and piperidine (40 μL, 0.40 mmol), and the mixture was stirred for 2 h at room temperature. Removal of the volatiles under reduced pressure followed by preparative TLC separation (silica gel; CH_2Cl_2–MeOH = 8.5:1) gave **14a** (54 mg, 0.080 mmol, 57% yield) as orange crystals. **14a**: δ_C (CD_3CN) 169.3 (C═O), 150.2, 137.2, 132.6, 132.5, 131.4, 129.9, 113.2, 112.8 (Ar + quart. C), 89.8, 87.8, 54.7, 51.2, 47.5 (η^6-Ar), 41.0, 40.8, 40.7 (NMe_2), 55.5, 52.6, 28.9, 28.8, 24.5 (piperidine). IR: 1612, 1567 (ν_{CO}), 1578, 1348 cm^{-1}. ESI-MS: 639 (**14a**−Cl), 554 (**14a**−Cl−piperidine) [20].

4.12. Preparation of *14b*

To crude **12** (163 mg, 0.138 mmol) were added CH_2Cl_2 (8 mL) and PEt_3 (75 μL, 0.51 mmol), and the mixture was stirred for 2 h at room temperature. Removal of the volatiles under reduced pressure followed by preparative TLC separation (silica gel; CH_2Cl_2–MeOH = 20:1) gave **14b** (88 mg, 0.124 mmol, 47% yield) as orange crystals. **14b**: δ_C ($CDCl_3$) 169.6, 149.7, 149.0, 131.5, 131.1, 129.4, 128.9, 112.6, 112.5, 88.5, 81.8, 72.0, 71.5, 42.5, 40.6, 40.41, 40.38, 15.3, 15.0, 8.10, 8.06. δ_P ($CDCl_3$; H_3PO_4) 20.0. IR: 1612, 1578, 1570 (ν_{CO}), 1348 cm^{-1} [20].

4.13. Preparation of *16*

A MeOH solution (20 mL) containing **15** (135 mg, 0.504 mmol) and **3** (148 mg, 0.464 mmol) was stirred

Table 4
Crystallographic data

Complex solvate	**5a** · $PF_6(CH_2Cl_2)_{0.5}$	**5b** · PF_6	**5a′** · PF_6	**6a**	**6b**	**7** · PF_6	**8** · $(PF_6)_2(CH_2Cl_2)_2$	**13a**	**14a′** · $(MeCN)_2$
Formula	$C_{24.5}H_{31}N_3F_6PCl$	$RuC_{24}H_{30}N_3F_6PRu$	$C_{34}H_{34}N_3F_6PRu$	$C_{17}H_{15}N_3O_3Cr$	$C_{17}H_{15}N_3O_3Cr$	$C_{36}H_{44}N_3O_2F_6PRu$	$C_{48}H_{63}N_3O_2F_{12}P_2Cl_4Ru_2$	$C_{31}H_{40}N_4O_2Cl_2Ru$	$C_{37}H_{50}N_7O_2ClRu$
Formula weight	649.02	606.56	730.70	361.32	361.32	796.80	1347.92	672.66	761.37
Crystal system	Monoclinic	Monoclinic	Orthorhombic	Triclinic	Triclinic	Orthorhombic	Triclinic	Monoclinic	Monoclinic
Space group	*C*2/*c*	$P2_1/c$	$Pca2_1$	$P\bar{1}$	$P\bar{1}$	*Pbcm*	$P\bar{1}$	$P2_1/n$	$P2_1/c$
a (Å)	26.003(2)	10.5359(6)	39.33(1)	6.17(2)	7.602(2)	7.711(1)	11.1283(3)	14.97(1)	10.732(1)
b (Å)	15.421(1)	14.519(1)	7.586(1)	15.79(4)	17.396(6)	21.464(2)	13.8350(9)	13.02(1)	27.247(4)
c (Å)	13.880(1)	16.605(2)	10.993(3)	17.58(5)	6.240(2)	21.171(2)	18.609(1)	15.96(1)	12.608(1)
α (°)	90	90	90	107.93(9)	99.60(2)	90	102.549(2)	90	90
β (°)	104.963(3)	90.984(4)	90	97.89(10)	95.66(2)	90	94.029(3)	92.48(5)	101.340(8)
γ (°)	90	90	90	91.45(10)	87.72(3)	90	91.621(3)	90	90
V (Å^3)	5376.9(8)	2539.7(3)	3279(1)	1610(7)	809.5(4)	3504.0(7)	2786.9(3)	3107(4)	3614.8(7)
Z	8	4	4	4	2	4	2	4	4
Temperature (°C)	−60	−60	25	−60	25	−60	−60	−60	−60
d_{calc} (g cm^{-3})	1.603	1.586	1.480	1.490	1.482	1.510	1.606	1.438	1.399
μ (mm^{-1})	0.803	0.742	0.589	0.731	0.727	0.562	0.871	0.711	0.551
Number of diffractions collected	17137	19554	3960	3773	3985	21718	21707	18663	25250
Number of variable	330	323	406	433	219	244	655	361	430
R_1 for data with $[I > 2\sigma(I)]$	0.0700 (for 3984 data)	0.0500 (for 4188 data)	0.0445 (for 2362 data)	0.0716 (for 1155 data)	0.0625 (for 2322 data)	0.0915 (for 2750 data)	0.0457 (for 9190 data)	0.0880 (for 1553 data)	0.0589 (for 6212 data)
wR_2	0.1885 (for all 5943 data)	0.1366 (for all 5734 data)	0.1502 (for 3960 data)	0.2254 (for all 3192 data)	0.1905 (for all 2848 data)	0.2231 (for all 4028 data)	0.1419 (for all 11278 data)	0.2773 (for all 6287 data)	0.1699 (for all 7436 data)

overnight at ambient temperature, and then the volatiles were removed under reduced pressure. To the residue was added acetone (35 mL) and the mixture was stand overnight at −30 °C. Removal of the supernatant solution gave **16** (207 mg, 0.374 mmol, yield 81%) as cream-yellow powders. **16**: δ_C ($CDCl_3$) 169.5, 159.0, 151.3, 147.7, 134.4, 130.1, 129.8, 127.3, 126.0, 125.5, 124.2, 115.8 (Ar + quart. C), 92.7 (C_5Me_5). 97.7, 89.2, 84.8, 83.2 (η^6-Ar), 10.1 ($C_5\mathit{Me}_5$). IR (KBr) 1769 cm^{-1} (ν_{CO}). ESI-MS: 555 (**16**). UV (CH_2Cl_2): λ_{max}/nm ($\varepsilon/M^{-1}\,cm^{-1}$) 310 ($1.9\times10^3$) [20].

4.14. X-ray crystallography

Single crystals were mounted on glass fibers. Diffraction measurements except for **5a**′ · PF_6 and **6b** were made on a Rigaku RAXIS IV imaging plate area detector with Mo Kα radiation ($\lambda = 0.71069$ Å) at −60 °C. Indexing was performed from two oscillation images, which were exposed for 5 min. The crystal-to-detector distance was 110 mm ($2\theta_{max} = 55°$). In the reduction of data, Lorentz and polarization corrections and empirical absorption corrections were made [21]. Crystallographic data and results of structure refinements are listed in Table 4.

Diffraction measurements of **5a**′ · PF_6 and **6b** were made on a Rigaku AFC5R automated four-circle diffractometer at 25 °C by using graphite-monochromated Mo Kα radiation ($\lambda = 0.71069$ Å). The unit cells were determined and refined by a least-squares method using 20 independent reflections ($2\theta \sim 20°$). Data were collected with ω–2θ scan technique. If $\sigma(F)/F$ was more than 0.1, a scan was repeated up to three times and the results were added to the first scan. Three standard reflections were monitored at every 150 measurements. In the reduction of data, Lorentz and polarization corrections were made. An empirical absorption correction (Ψ scan) was made.

The structures were solved by a combination of the direct methods (SHELXS-86 [22]) and Fourier synthesis (DIRDIF-94 [23]). Least-squares refinements were carried out using SHELXL-97 [22] (refined on F^2) linked to teXsan. All non-hydrogen atoms were refined anisotropically. Hydrogen atoms were fixed at the calculated positions unless otherwise stated. Crystallographic data for the structural analysis have been deposited at the Cambridge Crystallographic Data Centre: CCDC 608223 (**5a** · PF_6), 608224 (**5a**′ · PF_6), 608225 (**5b** · PF_6), 608226 (**6a**), 608227 (**6b**), 608228 (**7** · PF_6), 608229 (**8** · $(PF_6)_2$), 608230 (**13a**), and 608231 (**14a**′). Details of the refinements are as follows: **5b** · PF_6: The methyl hydrogen atoms were refined with the riding models. **6a**: A unit cell contained two independent molecules. **7**: The molecule sat on a crystallographic mirror plane and was disordered with respect to the Ru1–C11–C1–O1 plane. The occupancy of C2 and O2 was 0.5 and the hydrogen atom attached to C22 was not included in the refinement. **8**: One of the two CH_2Cl_2 solvate molecules was found to be disordered and refined by taking into account the minor component (Cl3–C62–Cl4:Cl3a–C62a–Cl4a = 0.52:0.48). The disordered parts were refined isotropically. **14a**′: The piperidine moiety was found to be disordered and refined by taking into account the minor component (0.527:0.423). The H0 and H1 atoms were refined isotropically and hydrogen atoms attached to the piperidine carbon atoms were not included in the refinement. The MeCN solvate molecules were refined isotropically.

Acknowledgement

This work was supported by the Grant-in-Aid for Scientific Research on Priority Areas (No. 16033219, "Reaction Control of Dynamic Complexes") from Ministry of Education, Culture, Sports, Science and Technology, Japan.

References

[1] M. Schwartz (Ed.), Encyclopedia of Smart Materials, Wiley, New York, 2002.
[2] C.O. Oriakhi (Ed.), Encyclopedia of Smart Materials, Wiley, New York, 2002, p. 172.
[3] A. Moriuchi, K. Uchida, A. Inagaki, M. Akita, Organometallics 24 (2005) 6382;
K. Takano, A. Inagaki, M. Akita, Chem. Lett. 35 (2006) 434.
[4] M.A. Bennett, K. Khan, E. Wenger, in: E.W. Abel, F.G.A. Stone, G. Wilkinson (Eds.), Comprehensive Organometallic Chemistry II, vol. 7, Pergamon Press, Oxford, 1995 (Chapter 8).
[5] M.J. Morris, E.W. Abel, in: F.G.A. Stone, G. Wilkinson (Eds.), Comprehensive Organometallic Chemistry II, vol. 5, Pergamon Press, Oxford, 1995 (Chapter 8);
A.D. Hunter, V. Mozol, S.D. Tsai, Organometallics 11 (1992) 2251.
[6] E.P. Kündig (Ed.), Transition Metal Arene π-Complexes in Organic Synthesis and Catalysis, Springer, Berlin, 2004;
H. Le Bozec, D. Touchard, P.H. Dixneuf, Adv. Organomet. Chem. 29 (1989) 163;
R.M. Moriarty, U.S. Gill, Y.-Y. Ku, J. Organomet. Chem. 350 (1988) 157.
[7] M. Hojo, T. Ueda, K. Kawamura, M. Yamazaki, Bull. Chem. Soc. Jpn. 73 (2000) 347;
G. Rihs, C. Weis, Dyes Pigments 15 (1991) 107.
[8] B. Steinmetz, W.A. Schenk, Organometallics 18 (1999) 943.
[9] We also examined reaction of the related rhodamine B and confirmed formation of the analogous 1:1 adduct (α ring adduct).
[10] C. Theocharis, W. Jones, J. Crystallogr. Spectrosc. Res. 14 (1984) 121.
[11] G. Bodes, F. Heinemann, G. Marconi, S. Neumann, U. Zenneck, J. Organomet. Chem. 641 (2002) 90.
[12] H. Werner, R. Werner, Chem. Ber. 115 (1982) 3766;
M.A. Bennett, A. Smith, J. Chem. Soc., Dalton Trans. (1974) 3011.
[13] M.A. Bennett, T.-N. Huang, T.W. Matheson, A.K. Smith, Inorg. Synth. 21 (1982) 74.
[14] M.A. Bennett, H. Neumann, M. Thomas, X.Q. Wang, P. Pertici, P. Salvadori, G. Vitulli, Organometallics (1991) 3237.
[15] R.H. Crabtree, The Organometallic Chemistry of the Transition Metals, fourth ed., Wiley, New York, 2005.
[16] The 1:2 adduct, $[(\eta^6\text{-PP})(RuCp^*)_2](PF_6)_2$, was obtained by the reaction of **3** with an excess amount of **4** · PF_6 and was characterized by its spectral data. The two α rings of the open form are coordinated by the $RuCp^{*+}$ fragments. δ_H ($CDCl_3$) 8.05 (1H, d, 6.3), 7.75–7.66 (2H, m), 7.52 (2H, d, 6.7) (Ar), 5.36 (2H, d, 8.4), 5.03 (2H, d, 8.4), 4.60 (1H, d, 8.4), 4.53 (2H, d, 8.4) (η^6-Ar), 1.69 (Cp^*); δ_C ($CDCl_3$) 168.2 (C=O), 150.7, 134.5, 131.1, 126.1, 124.6, 123.8 (Ar), 95.3 (C_5Me_5), 91.7, 87.2, 83.8, 82.3, 76.5, 76.3 (η^6-Ar), 9.7 ($C_5\mathit{Me}_5$); IR: 1773 cm^{-1} (ν_{CO}).
[17] T. Kanbara, M. Oshima, T. Imayasu, K. Hasegawa, Macromolecules 31 (1998) 8725.

[18] M.O. Albers, T.V. Ashworth, H.E. Oosthuizen, E. Singleton, Inorg. Synth. 26 (1989) 68;
P. Powell, J. Organomet. Chem. 65 (1974) 89, see also, Ref. [14].
[19] S.D. Loren, B.K. Campion, R.H. Heyn, T.D. Tilley, B.E. Bursten, K.W. Luth, J. Am. Chem. Soc. 111 (1989) 4712.
[20] Despite several attempts analytically pure samples could not be obtained.
[21] T. Higashi, Program for Absorption Correction, Rigaku Corp., Tokyo, Japan, 1995.
[22] (a) G.M. Sheldrick, SHELXS-86: Program for Crystal Structure Determination, University of Göttingen, Göttingen, Germany, 1986; (b) G.M. Sheldrick, SHELXL-97: Program for Crystal Structure Refinement, University of Göttingen, Göttingen, Germany, 1997.
[23] P.T. Beurskens, G. Admiraal, G. Beurskens, W.P. Bosman, S. Garcia-Granda, R.O. Gould, J.M.M. Smits, C. Smykalla, The DIRDIF Program System, Technical Report of the Crystallography Laboratory, University of Nijmegen, Nijmegen, The Netherland, 1992.